WILEY-VCH

DOI: 10.1002/ ((please add manuscript number))
Article type: Review

Bioinspired Surfaces with Superwettability for Anti-icing & Ice-phobic Application: Concept, Mechanism, and Design

*Songnan Zhang, Jianying Huang, Yan Cheng, Hui Yang and Yuekun Lai**

S. N. Zhang, Prof. J. Y. Huang, Y. Cheng, H. Yang, Prof. Y. K. Lai
National Engineering Laboratory for Modern Silk, College of Textile and Clothing Engineering, Soochow University, Suzhou 215123, P. R. China
E-mail: yklai@suda.edu.cn

Keywords: wettability, anti-icing, ice-phobic, superhydrophobic surface (SHS), slippery liquid-infused porous surface (SLIPS)

Abstract: Nowadays, ice accumulation has brought a series of severe issues in daily life. Bioinspired from the nature, i.e. lotus leaf, cicada wing, mosquito eyes, Nepenthes alata, superwettability surfaces have attracted great interests from fundamental research to anti-icing & ice-phobic Application. Here, recent published literatures about the mechanism of ice prevention have been reviewed, with a focus on the anti-icing mechanism and ice-phobic mechanism, which involve in the process of freezing, consisting of condensate microdrops self-propelling, drops bouncing, wetting, ice nucleation and freezing. Then, a detailed account of the innovative fabrication and further fundamental research of anti-icing materials with special wetting are summarized with highlight on the recent progress and comparison, i.e. low-surface energy coatings and liquid-infused layered coatings. Finally, special attentions are paid on discussion about advantages and disadvantages of the technologies, as well as factors that affect the efficiency of anti-icing & ice-phobic. Present outlooks and the current

challenges for future development of the anti-icing and ice-phobic technology are presented and discussed.

1. Introduction

During cold weather, ice accumulating on solid surfaces can cause serious problems on roads,[1-13] aircrafts,[14-28] power lines,[29-32] ships, and some energy equipment. As for roadway accidents that is directly related to roadway and weather conditions, related statistics indicate that thousands of human injuries and deaths and millions of dollars in property damage annually happened, which accounts for ten to fifteen percent of all roadway accidents. Ice accumulation is not only a concern for chauffeurs on the highway, but also accounts for personal injuries on walkways due to numerous slipping and falling.[1-13] Especially when ice accumulate on the wings of aircraft and turbine engine structures or insulators and transmission lines on power systems, it will impose serious problems and cause some disastrous damage in the aircraft industry and power industry.[14-32] In the winter of 2008-2009, frozen rain lasted for more than three weeks in Hunan and Jiangxi provinces, causing that thirty-seven percent of the 500 kV power transmission towers were brought down. Therefore, researchers around the world have paid more attention to ice prevention technology and devoted themselves to a large number of scientific research principle of ice.

In the past decades, several anti-icing methods have been developed to reduce the ice formation and improve the ice-phobic ability on structures. Traditional prevention methods of ice accumulation are mostly based on the thought of deicing or melting ice,

giving priority to thermal de-icing, mechanical de-icing and other passive de-icing methods, which can't solve the problem fundamentally and produce large amounts of energy consumption. Energy and environmental issues are the focus of the world today, Therefore, how to save energy and avoid the pollution of environment should be considered. Due to several drawbacks of the commonly used ice removal strategies, ice prevention coatings gradually become the research focus, which is designed to suppress or delay the formation of ice crystals on the material surface, reduce the ice crystals of matrix adhesion, and possess the advantage of less energy consumption, environment friendly, and wide applicability. As for ice prevention coatings, prevention and control of ice accumulation on solid surfaces are the critical factors to fabricate the functional materials with anti-icing and ice-phobic ability. Excellent ice prevention coatings can not only reduce ice-adhesion, but also delay water freezing on surfaces, which causes lower ice accumulation on such coated surfaces.[33]

To develop functional materials for ice prevention, it is essential to first understand the ice prevention mechanisms before the functional materials are developed. Therefore, it is the purpose of this review to present the latest understanding and technology for artificial ice prevention materials. In this review, the mechanisms of ice prevention are firstly categorized into two aspects, the one is theory of anti-icing, the other one is theory of ice-phobic. As for theory of anti-icing, we introduce the mechanism of condensate microdrops self-propelling, drops bouncing and wetting in detail. As for theory of ice-phobic, ice nucleation mechanism and ice adhesion mechanism are demonstrated in detail. In the second part, we focus on the published literatures to

introduce the fabrication and further fundamental research of anti-icing materials, dividing them into three parts, that is low-surface energy coatings, liquid-infused layered coatings with highlight on the recent progress and comparison. Finally, special attentions are paid on discussion about advantages and disadvantages of the technologies, and we draw conclusions and present outlooks for future development of the anti-icing and ice-phobic technology.

2. The mechanisms of anti-icing & ice-phobic

Bioinspired by the nature, i.e. lotus leaf,[34] cicada wing,[35] mosquito eyes,[36] Nepenthes alata,[37] butterfly,[38] rice leaf etc.,[39] more and more investigation are carried out by researchers.[40-42] Bionic superhydrophobic and low-adhesion materials have received substantial attention by researchers.[43-48] As shown in **Figure 1**, creatures possess special natural adaptability due to the unique structure and surface mass, such as the lotus leaf and cicada wing which possess the ability of self-cleaning, the mosquito which have the ability of anti-fogging, the Nepenthes alata which can collect water, and the butterfly and rice leaf which can achieve the direction of water droplets. Over the past decade, theoretical research on anti-icing and ice-phobic has made significant progress. As for research on anti-icing and ice-phobic, understanding their mechanism is significant to guide practice. **Figure 2** shows the process of freezing, that is self-propelling, bouncing, wetting, nucleating and bridging, which involves the phase of liquid and solid. In the stage of liquid, the anti-icing ability should be considered; In the stage of solid, the ice-phobic ability should be considered. As for theory of anti-

icing, mechanism of condensate microdrops self-propelling, drop bouncing and wetting are demonstrated below. As for ice-phobic, we demonstrate the mechanism of ice nucleation and adhesion in detail.

2.1. Theory of anti-icing

2.1.1. Droplets self-propelling mechanism

Bioinspired by the phenomenon occurring commonly on the creature, such as cicada wing and water-strider,[49, 50] most research on anti-icing has focused on coalescence-induced self-propelling drops because of its value of potential applications. Nevertheless, the mechanism of self-propelling remains poorly understood, including the factors of self-propelling efficiency.[51-53]

As an efficient type of propelling, the condensate microdrop self-propelling (CMDSP) results from the surface energy released upon drop coalescence-induced without the action of any external forces, which has the widely potential application.[54] Yao et al. has verified that the frequency of CMDSP is significantly affected by the surface roughness, the chemical properties, and the superhydrophobicity stability under dew condensation. The nanostructures with sufficiently narrow spacing, higher perpendicularity, and lower surface energy would contribute to the enhanced drop mobility owing to less pinning of the condensate drops.[55] Herein, contact line[56] (**Figure 3A**) and contact line distortion[57] (Figure 3B) should be mentioned due to the significance of contact mode, because they play the key role in the dynamic droplet models, including advancing, pinning and receding modes.[56-59] Thereby, through a

series of experiments, Zhang et al. verified that hydrophilic defect sites are beneficial to nucleation and hydrophobic coatings contribute to self-propelling as shown in Figure 3C.[60] When droplets condensed on the substrate, the self-propelling dynamics of coalescence-induced microdrops obey the equation:[60-65]

$$E_{itk} = \frac{1}{2} m {V_e}^2 = \Delta E_s - \Delta E_{int} - \Delta E_h - \Delta E_{vis} \qquad (1)$$

Where ΔE_s, E_{int}, ΔE_h stand for the released surface energy, interfacial adhesion-induced dissipation energy, and the gravity potential energy, respectively. The viscous dissipation (ΔE_{vis}) may be ignored in the coalescence-induced self-propelling process unless droplets are very small (<500 nm), as verified by Wang et al.[62] In Equation (1), m represents the mass of the drop after coalescence and V_e (the average velocity) is given by

$$V_e = \frac{1}{5} U = \frac{1}{5} \sqrt{\frac{\sigma_{LV}}{\rho R}} \qquad (2)$$

Where σ_{LV}, ρ stand for liquid–vapor interface tension and water density, respectively, R stands for of the radius of merged microdrop. ΔE_s and ΔE_h are given in Equation (3) and (4) below, where r stands for the radius of the microdrop before coalescence, ΔA and V stand for the difference of surface area and the volume of the merged microdrop, respectively, θ stands for the contact angle.

$$\Delta E_s = \sigma_{lv} \Delta A \qquad (3)$$

$$\Delta E_h = mg\Delta h = mg \left[\left(\frac{3V}{4\pi} \right)^{\frac{1}{3}} - \frac{r(3+\cos\theta)(1-\cos\theta)}{4(2+\cos\theta)} \right] \qquad (4)$$

By showing a full 3D numerical model to analyze the motion of coalescence-induced on SHS surfaces, Nam et al. investigated that approximately half (40-60%) of the released surface energy was transformed into kinetic energy during the process of coalescence.[66] Whereas, Wang and her coworkers combined detailed measurements of CMDSP with numerical simulations of droplets coalescence, and thought this process is fundamentally inefficient with less than 6% of the excess surface energy convertible into translational kinetic energy, which demonstrated the role of internal fluid dynamics during the coalescence process of jumping droplet and underpin the development of systems that can harness jumping droplets.[62] Additionally, they thought overcoming energy barriers would cause the occurrence of wetting states through nucleation-mediated droplet-droplet interactions, which offers insight into the role of optimized surfaces designing.[51] Herein, by controlling the roughness, tailoring bionic nanofilms, sharpening the nanostructures, or designing proper surfaces are necessary to achieve the desired CMDSP functional surface.[67-78] Recent observations verified that hierarchical SHS possess an excellent property of CMDSP.[60, 70, 79-81] Through a series of experiments, Zhang et al. investigated that hierarchical SHS possess the most excellent CMDSP property compared to nano-structured surfaces. Meantime, they stated that the value of surface of adhesion affected the motion of self-propelling at a certain extent, including the velocity of self-propelling and critical size.[81, 82] However, theoretical analysis reveals that a critical size of about 10 μm occurs in the process of self-propelling.[65]

As for the suspend droplets, to achieve effective dropwise condensation and the property of anti-icing, condensate must be quickly removed from the surface due to its accumulation. But as for the partial droplet, to restrain condensation growth rates for Cassie stable surfaces before freezing, controlling the droplet wetting morphology is very significant. Due to the droplets' increased contact with the substrate during the process of condensation, the initial growth rate of the partial wetting morphology was higher than that of the suspend morphology.[83] Herein, as for partial wetting morphology, delaying growth of ice nucleation and reducing the ice adhesion will be a second approach,[84-89] which will be introduced in the next part.

2.1.2. Drops bouncing mechanism

To resist icing, surfaces should be designed that drops do not cling to them but bounce off, and ensured the contact time is short.[90-93] A drop bouncing on a non-wetting surface will experience two stages, the first is dropping down on the surface and spreading out to a maximum diameter, the second is recoiling to an extent that it completely rebounds and leaving the surface.[94] Drops bouncing performance on a dry solid surface depends on the surface roughness, wettability, temperature of the substrate, and the ambient conditions.[95-102]

Nowadays, we measure the values of the relevant dimensionless parameters to position our experiments within the extensive experimental work on droplet impact. Herein, Schiaffino and Sonin stated a useful approach and distinguished four impact regimes by using three dimensionless parameters.[103] The first is the Weber number (We), which represents the ratio of the inertial force and surface tension. The smaller

of the Weber number represents that the surface tension is more important, once the Weber number is greater than 1.0, the effect of surface tension can be ignored. The second is the Reynolds number (Re), which stands for the ratio of inertia force and viscosity. The smaller of the Reynolds number means that the viscosity have the more significant effect, conversely means that the inertia have the more significant influence. The third is the Ohnesorge number (Oh), which are used rarely. Relevant equation are listed below. Herein, the liquid drop of density, diameter, and impact velocity are abbreviated by ρ, D_0, and v, respectively, and surface tension and dynamic viscosity are γ and μ, respectively.

$$We = \frac{\rho v^2 D_0}{\gamma} \qquad (5)$$

$$\mathrm{Re} = \frac{\rho v D_0}{\mu} \qquad (6)$$

$$\mathrm{Oh} = \frac{\mu}{\sqrt{D_0 \sigma \rho}} \qquad (7)$$

Especially, drops partially or fully pin, or splash depends on their velocity and viscosity.[104-106] As for low Weber number, the droplet impact is quasi-elastic with a small-scale deformation because of negligible energy dissipation. As for large We and Re, the droplet splash occured with disintegrating into two or more secondary droplets.[95, 97, 103, 106] Based on the dimensionless parameters,[104, 105, 107-112] we concluded that the kinetic energy of the impinging drop dissipated by viscosity during the impact in the viscous-inertial system,[108] the maximum diameter yields $D_{max} \sim D_0 Re^{1/5}$.[113, 114] As for viscous drops, Schroll et al. simiulated the impact of a viscous liquid drop onto a smooth dry solid surface. When the ambient air pressure is reduced to a very low value, impact at several m/s flattens the falling drop without producing a

splash, which reveals that the thin, spatially uniform pancake shape that a falling drop gets flattened into owes its existence to the boundary layer in the liquid drop created by impact.[111] Meanwhile, the lamella ejection is limited by the impact velocity and liquid viscosity.[110] In the capillary-inertial system, the kinetic energy of the imping drop can be transfered into surface energy purely,[115] the maximum diameter yields D_{max}~ $D_0We^{1/2}$ or $We^{1/4}$.[108] Recently, Visser et al. found that no splashing was observed with droplet diameters between 12 and 100 μm for all impact at velocities up to 100 m s^{-1}. Compared with several models, they found the measured data agreed with the model by Pasandideh-Fard et al.[116], which indicated that boundary layer dynamics have a key effect on droplet spreading. Meanwhile, due to the using of an initial contact angle of 180 degrees as the model input value, they confirmed the presence of an air layer under the impacting droplet, which verified by Jolet de Ruiter et al., they introduced a different universal bouncing mechanism that an air film for moderate drop impact velocities can occur continuously on both wetting and non-wetting surfaces.[109]

As for bouncing drop, the contact time, that is the time period from the start of a drop impacting to the end of bouncing off the substrates, is the most important parameters to characterize the drop dynamic. In 2002, Quéré's group measured the duration of the drop remaining in contact with the substrate, and quantify the efficiency of SHS.[115] As for the drop impacting on SHS, we consider its inertial-capillary nature to simplify, and viscosity is not important here. By balancing inertia ($\rho R/\tau^2$) with capillarity (γ/R^2), the contact time is:[115, 117]

$$\tau \approx \sqrt[2]{\frac{\rho R^3}{\gamma}} \qquad (8)$$

From the equation, we can find that τ mainly depended on the drop radius, which also can be found from the **Figure 4A**, it was well fitted by $R^{3/2}$ with a wide range of radius (0.1-4.0 mm), and not depended on the impact with a wide range of velocities (20-230 cm s^{-1}) but increased with the range below 10 cm s^{-1}, which could be due to the drop's weight.[115, 117]

Notably, different from the minority of the contact time in the inertia-dominant spreading stage, the time of retracting stages nearly accounts for 70-80% of the total contact time. Denis Bartolo et al. identified two regimes for the retraction rate: a viscous regime and an inertial regime. Viscous force and surface tension forces determine the drop retraction rate (V_{ret}/D_{max}).[118] For the inertial regime, based on the Taylor–Culick approach,[119, 120] the retraction rate follws Equation (9), where τ_i means the inertial time, θ_r stands for the receding contact angle; For the viscous regime, the retration rate follows Equation (10).[97, 118]

$$\frac{V_{ret}}{R_{max}} \sim \frac{\sqrt{1-\cos\theta_r}}{\tau_i} \qquad (9)$$

$$\frac{V_{ret}}{R_{max}} \sim \frac{\mu R_0}{\gamma} \qquad (10)$$

Therefore, how to reduce the contact time is significant to anti-ice, as for that, some researchers found that wetting hysteresis and the solid fraction play significant roles in determining the duration between impacting and bouncing off the substrate.[121, 122] James et al. used SHS with a morphology to redistribute the liquid mass and reduce the contact time.[94] Qué é think that under the presence of macrotextures, the

hydrodynamics are changed significantly, which is a significant step in the maximization of water repellency and the minimization of the contact between solid and liquid.[123] The spreading and retracting time consists the overal contact time. Shen et al. found that the entire water drop was divided into two, three or more parts due to the assistance of the "cross-shaped" surface macrotextures, thereby the retracting process of the impacting can be entirely integrated into the process of spreading out to the maximal deformation, which results that contact time was shorten and created a contact time limitation of 5.5 ms from Figure 4B.[124] Meanwhile, Wang's group investigated that pancake bouncing on SHS could have a fourfold reduction in contact time, which is due to the rectification of capillary energy stored in the penetrated liquid into upward motion adequate to lift the drop. Compared to the conventional complete rebound, pancake bouncing experienced the liquid penetration deeper and detaching from the surface without experiencing retraction.[125] Thereby, their group found that water droplet displayed asymmetric bouncing dynamics with different spreading and retraction along two directions when the drop impacted on Echevaria leaves, which resulted from the concave/convex architecture of cylindrical leaves.Through further experiments on mimetic surfaces and lattice Boltzmann simulations, they conclued that preferential fluid pumping around the drop rim created asymmetric momentum and mass distribution, which leaded to ~40% reduction in contact time.[126]

However, irreversible transiton between Cassie and Wenzel will bring the loss of the anti-adhesive performances realated with superhydrophobicity, and have a bad effect on the anti-icing property.[127-137] However, the mechanism of Cassie-Wenzel

transition is still hanging in debate, the universal illustration is that the pressure is present in the bouncing process. As considered by Quéré's group,[133] how to avoid an irreversible transition is lying on the design of superhydrophobic materials.[128] They demonstrated that because of two levels of texture on hierarchical structure, the SHS indeed had a large roughness. This structure didn't strengthen the hydrophobicity, but also stabilized the Cassie regime and water repellency. Thereby, they discussed the conditions that how the surface design could fulfill a water droplet bouncing off without satellite ejection, and investigated that the critical value of satellite ejection is about 160 of We number, which is lower than that of hydrophobic flat surface (We number of 700) and hydrophilic surface (We number ＞1000). Meanwhile, they emphasized the role of the film of air in minimizing the viscous dissipation, and stated the conditions of pinning occurring if the velocity satisfied the inequality,[134] where h and l stands for the height and distance of micro-pillars, V^* represents the critical velocity.

$$V > V^* = \sqrt{\frac{\gamma h}{\rho l^2}} \qquad (11)$$

And soon afterwards, Bartolo et al. verified the equation that the dynamic pressure (P_D) acting on the liquid interface through gathering static and impact experimental data. If the dynamic pressure (P_D) exceeds capillary pressure (P_C), the transiton of Cassie-Wenzel inevitably occured.[127]

$$P_D = \frac{1}{2}\rho V_1^2 \qquad (12)$$

$$P_c = \frac{\sigma}{a}\left[\frac{-4\cos\theta_a}{\left(1+\frac{b}{a}\right)^2 - 1}\right] \qquad (13)$$

where θ_a is the advancing contact angle on a smooth surface, a is the post width, and b is the spacing between posts. Meanwhile, they reported three distinct regime, that is fakir droplet regime (for the impact velocity small enough), bouncing droplet regime (for the intermediate impact velocities), and sticky droplet regime (for high impact velocities). Thereby, by using the lattice Boltzmann method, Hyv ädluoma and Timonen confirmed Bartolo et al.'s research and find a fourth possible regime that a non-bouncing ends up in the fakir state (for impact velocities lager than those for bouncing drops but smaller than those for sticky drops).[131] Different from the Bartolo et al.'s research, researchers found that the calculated anti-wetting capillary pressure (P_C) far exceeded the value of calculated dynamic pressure (P_D) by using the equation (12) and (13), which can't explain the wetting transition,[137] then they further demonstrated the significant role of water hammer pressure (P_{WH}) in the transition of the droplet to the Wenzel state.[129, 130, 137] Therefore, the water hammer pressure (P_{WH} obeys the Equation 14) was created and explained by producing at the contact area with a radius (R_{WH} obeys the Equation 15). Where k stands for a constant determined by the type of impacting surface, shape, and velocity of the droplet, C stands for the speed of sound, R_0 stands for the initial droplet radius. With the presence of the water hammer pressure (P_{WH}), Deng's group clearly defined three wetting states for the impinging droplet, that is total wetting state ($P_{WH} > P_D > P_C$), partial wetting state ($P_{WH} > P_C > P_D$), and total non-wetting state ($P_C > P_{WH} > P_D$), which is shown in Figure 4C.[129] In a word, the transition from the Cassie regime to the Wenzel regime depends on the intergration

between impact velocity, geometric parameter, materials and liquid properties.[130, 132, 136]

$$P_{WH} = k\rho VC \qquad (14)$$

$$R_{WH} = \frac{R_0 V}{C} \qquad (15)$$

Notably, when droplet bouncing on the substrate, how to control the direction is vital to the transportation of the droplets.[138-142] Using the decorated substrates with a texture of variable density, Quéré's group investigated the impacting water drops bouncing off obliquely and verified the transition mechanism of bouncing direction that the asymmetric would lead to a transportation of the liquid towards fields of high texture density.[141] By engineering nonuniform textures to create roughness gradients on the substrate, Wang's group achieved the gradient surface, where the droplet can be controlled to rebound axially and rebound by a prescribed lateral trajectory.[140] Additionally, they investigated that the self-migration direction (toward or against the wettability gradient) maily depended on the competition of the capillary pressure and the effective water hammer pressure, which is different from the previous reports,[142] and is significant for some potential applications, such as anti-fogging, water-harvesting and anti-icing. As for transportation of microdrops (scale of μm) , we will summarize that in detail at the next part.

2.1.3. Wetting mechanism

If a droplet of liquid is placed on a smooth solid surface, the wettability of the surface can be described using Young's equation (**Figure 5A**) as follows:[143]

$$\cos\theta = \frac{(\gamma_{SA} - \gamma_{SL})}{\gamma_{LA}} \qquad (16)$$

It involves the thermodynamic equilibrium contact angle θ of a drop on an ideal solid, the specific energies of the solid in air (γ_{SA}), the solid in liquid (γ_{SL}), and the liquid in air (γ_{LA}). This equation was firstly proposed by Young in 1805, but only applicable on the surfaces with physically smooth or chemically homogeneous. Considering the influence of roughness, heterogeneity etc., Wenzel and Cassie further propose their investigation on the apparent contact angles.

As shown in the Wenzel model (Figure 5B), the liquid is in contact with the solid surface and completely pins into the valleys of the rough surface. Wenzel firstly proposed the new model for rough surfaces in 1936, stating that a rough material has a higher surface area compared to a smooth one, and modifies the contact angles expression as follows:[144, 145]

$$\cos\theta^* = \mathrm{r}\cos\theta \tag{17}$$

where r is the surface roughness that is defined as the total surface area of structures divided by the projected surface area, θ* and θ are the CA of liquid droplet on the rough surface and the smooth surface of the same material, respectively. Among the parameters, θ can be described by Young's equation, and r·cosθ is limited within 1.

As shown in the Cassie model (Figure 5C), due to the air filling in these valleys, the liquid drop cannot pin into valleys on the rough surface. Cassie and Baxter first proposed the following equation for this model in 1944:[146]

$$\cos\theta^* = f_{SL}\cdot\cos\theta_1 + f_{LA}\cdot\cos\theta_2 \tag{18}$$

where f_{SL}, f_{LA} stand for the area fraction of the liquid droplet in contact with the solid surface, and the rough surface with air trapped in the valleys, respectively. θ_1 and θ_2

stand for the CA of liquid in contact with solid surface and air, respectively. For this rough surface, air trapped in the valleys can be considered completely non-wetting (θ_2 = 180° and $\theta_1 = \theta$), and $f_{SL} + f_{LA} = 1$. Therefore, the equation of Cassie model can be redefined as follows:[146]

$$\cos\theta^* = f_{SL}(\cos\theta + 1) - 1 \quad (19)$$

These are the two important models to describe the wettability behavior on rough surfaces used to explain the effect of roughness on the apparent contact angle of a liquid droplet on a rough solid surface. Together with Young's equation that explains the water contact of an ideally smooth surface, the three classical models have been widely applied for liquid contact in static state.

For dynamic wettability evaluation of a liquid-repellent surface, Furmidge proposed the Furmidge equation (Figure 5D) to explain the dynamic wettability as follows:[147]

$$mg\ sin\ \alpha = \sigma w(cos\ \theta_r - cos\ \theta_a) \quad (20)$$

where m, σ and w are the weight, surface tension and contact circle width of the liquid droplet, respectively, g is the gravitational acceleration, α the sliding angle (SA), and θa and θr the advancing contact angle (CA) and receding contact angle (CA), respectively. In the Furmidge equation, the significant characterization parameters are CA, SA or contact angle hysteresis (CAH, the difference between the advancing contact angle θa and receding contact angle θr). CA indicates that the degree of water-repellency of liquid on the solid surface; whereas a low SA or small CAH reveals that droplet has low adhesion and can slide readily on the surface.

For the Cassie model, the actual contact area is much smaller than the apparent area, and this will result in a small SA due to the low interaction area between liquid and solid surface. Contrariwise, for the Wenzel model, the actual contact area between the liquid droplet and solid surface is larger than the nominal area, therefore much greater interaction and larger SA are expected.

2.2. Theory of anti-icing & ice-phobic

Ice formation and accretion may happen everywhere, such as airplanes, roads, power lines and so on. Therefore, understanding the mechanism of ice nucleation and adhesion is of significance to the peoples' daily life.

2.2.1. Ice nucleation mechanism

Contrast to expected heterogeneous nucleation at the liquid–solid interface, Jung et al. verified that the freezing process started with homogeneous nucleation at the gas–liquid interface resulted from the evaporative cooling of the supercooled liquid as shown in **Figure 6A**. Humidity and the flow of a surrounding gas heavily affect surface ice-phobicity through switching the ice crystallization mechanism.[148] Under quasi steady-state conditions, the energy of evaporation equating the energy balance at the gas–liquid interface obeys the equation:

$$Q_v = Q_g + Q_w \qquad (21)$$

Which Q_g means the sum of the energy transferred by convection from the surrounding gas, Q_w means the heat conduction from the droplet bulk to the interface, But due to the allowance of enough time to cool down the droplet to the chamber and substrate

temperatures, we neglect the heat transfer at the solid–liquid interface before placing it on the substrate. In fact, we can estimate the local temperature differential at the gas–liquid interface of the water droplet as:

$$\Delta T = T_g - T_w \approx -\frac{\Delta H_v \xi \rho_w}{M r_0} \frac{1}{h_g + \frac{k_w}{l}} \qquad (22)$$

where ΔH_v, ρ_w, M, h_g, k_w, l, r_0 stand for the enthalpy of vapourization from water vapour, the density of liquid water, the molecular weight, the convective heat transfer coeffcient of gas water, the thermal conductivity of liquid water, the height and the initial radius of the droplet, respectively. The evaporation rate constant ξ was experimentally determined obey the equation:

$$\xi = \frac{D\rho_{v,\ sat}}{\rho_w}(1-\varphi) + C(1-\varphi) \qquad (23)$$

where D, $\rho_{v,\ sat}$, φ, C mean the diffusivity of water vapour in air, the saturated water vapour mass concentration at the gas–liquid interface, the influence of gas flow on the droplet, and the relative humidity, respectively.[148]

As reported by the previous research, how to restrain ice nucleation lies in two key respects: First is removing subcooled condensate microdrops continuously to prevent ice nucleation,[84] which has been demonstrated above. For intermediate supercooling temperatures, nucleation becomes the dominant factor controlling icing at the water−substrate interface, but not the dominant factor (bulk and air−water nucleation dominate) for lower supercooling temperatures.[149] Additionally, due to the low surface energy coupled with the rough surface and the Cassie wetting state, ice-phobic surfaces tend to lower the nucleating temperature better than the non-ice-phobic surfaces,[150]

Second is controlling the formation of inter-drop ice bridge to delay frost growth.[84] Different from other reports of condensation frosting, focusing exclusively on liquid-solid ice nucleation for isolated drops on SHS, such as deposited drops and impacting drops.[90, 93, 148, 149, 151-154] As shown in Figure 6B and 6C, Boreyko et al. developed a simple scaling model, and they investigated that the growth of frost was an interdrop phenomenon that is strongly coupled to the wettability and drop size distribution of the surface.[84] It seems unavoidable that the interdrop growth of frost form on the surface through subcooled condensate in humid environments. But Boreyko et al. took advantage of nanostructured SHS to promote the growth of frost in a suspended Cassie state, and achieved its dynamic removal through partial melting at low tilt angles (<15 °). The process of dynamic defrosting experienced two stages: gravitational mobilization and spontaneous dewetting, which minimizes the time, heat, and gravitational energy required to remove ice from the substrate as shown in Figure 6D.[155] However, the impurities in water and surface heterogeneities are uncontrollable factors that generate an obstacle for demonstrating the effects of surfaces on ice nucleation. Integrated the process of evaporation, condensation, and subsequent ice formation into a designed closed cell, Li et al. investigated the ice nucleation of ensembles of independent condensed water microdroplets on surfaces with completely different wettabilities, and found that the rate of ice nucleation on a hydrophobic surface is about 1 order of magnitude higher than that on a hydrophilic surface, which resulted from the difference in the surface roughness and the viscosity of interfacial water.[156, 157] As for the rate of nucleation J(t) related with the time (t), which can be expressed as:[158-160]

$$J(t) = -\frac{1}{N(t)}\frac{dN(t)}{dt} \qquad (24)$$

Where N(t) stands for the number of droplets that remain unfrozen after a time t. According to the classical nucleation theory,[161] the temperature-dependent (T) nucleation rate J(T) can be expressed as:

$$J(T) = J_0 exp\left[-\frac{\Gamma}{T(T_m - T)^2}\right] \qquad (25)$$

Where

$$\Gamma = \frac{16\pi f(\theta_{IW})\gamma_{IW}^3 v_i^2 T_m^2}{3kq^2} \qquad (26)$$

$$f(\theta_{IW}) = \frac{1}{4}(2 + \cos\theta_{IW})(1 - \cos\theta_{IW})^2 \qquad (27)$$

Where J_0 means the nucleation prefactor correlated with diffusion activation energy, f (θ_{IW}) means a wetting angle factor, Γ means the ice-water interfacial energy. γ_{IW}, v_i, T_m, k, q stand for the scaling factor, the specific volume of ice phase, the melting temperature of ice, Boltzmann's constant, the latent heat of fusion, respectively. Based on these theories, Li et al. developed a method to extract the thermodynamic parameters.[157] From these parameters, they verified that the nucleation rate depended on the viscosity of interfacial water, the nucleation prefactor was their evidence, which are extracted as:

$$J_0 \propto \left(\frac{\gamma_{SL}}{kT}\right)^{\frac{1}{2}}\left(\frac{h}{\eta v_m}\right) \qquad (28)$$

Where H, v_m, η represent Planck's constant, molecular volume, and the viscosity, respectively.

Experimentally, most of achievements reveal that frost formation or ice nucleation significantly compromises the ice-phobic properties of SHS,[162] that is the adhesion of ice nucleation, which will be discussed in the next section.

2.2.2. Ice adhesion mechanism

As for the characterization of ice-phobic, the adhesion of ice is a significant parameter to evaluate the property of ice-phobic surface. An excellent anti-icing & ice-phobic should possess two key characteristics, one is the ability of overcooled droplets rolling off the surface,[90-93] which is discussed in the above, the other one is the weaken ice adhesion of surface.[163-165]

Among several decades, most of researchers thought wettability has relationship with the ice adhesion. SHS was regarded as the most effective approach to fabricate anti-icing materials for some years. Dotan et al. investigated that the SHS surface possess the lowest ice adhesion owing to the highest contact angle. Additionally, they found that as for both extreme cases (hydrophobic and hydrophilic), low level of interactions lead to low ice adhesion for hydrophobic surface, and high level of interactions lead to high ice adhesion for hydrophilic surface.[166] However, diffent slightly from Dotan et al., Kulinich et al. show that ice adhesion had no correlation with contact angle for rough hydrophobic surfaces, instead of good correlation with wetting hysteresis due to the relationship with the ice-solid contact area, which is only effective to rough hydrophobic surfaces with low wetting hysteresis.[167] Furthermore, Meuler et al. investigated that the average strength of ice adhesion had strong correlation with the practical work of adhesion scaling parameter ($1+\cos\theta_{rec}$) for liquid water on smooth

surfaces, which suggested that measuring the receding contact angle is a method to evaluate the ice-phobic property of smooth surfaces.[168] Wang et al. investigated that the ice adhesion on this SHS was significantly reduced, which is made by a simple dip coating process. The ice adhesion on this SHS was reduced by the only 13% of that on the superhydrophilic surface due to the presence of an "air cushion" between the surface and water in the SHS. Compared to the superhydrophilic surface, the ice adhesion strength on SHS surface only slightly increased less than 20%, which revealed an excellent durability of the ice-phobic property.[169]

However, most researchers thought SHS cannot always reduce the ice adhesion,[170-174]and maybe the surface wettability cannot always predict the ice adhesion due to the complicated adhesion mechanism existing in liquid-solid and ice-solid systems.[175] Kulinich et al. found that when the rough morphology surface was gradually damaged during icing and deicing cycles (as shown in **Figure 7A**), ice-phobic properties of the materials are weakened. Additionally, when droplets condensed in the rough structure, the ice nucleation would occupy the surface asperities, which may lead to very large values of ice adhesion on such surfaces.[172] Meanwhile, Wang et al. investigated the impact of surface texture and wettability on the ice adhesion, and found that textured surfaces possessed high ice adhesion compared with the smooth surfaces, which revealed superhydrophobic didn't reduce the ice adhesion. Additionally, they verified that the ice adhesion increased linearly with the increase of the area fraction of air in contact with liquid.[171] To explore the reason that SHS are not always ice-phobic, Michael and Vahid used mechanical forces model to analyze the relationship of ice

adhesion with the receding CA and the initial size of interfacial cracks as shown in Figure 7B. They demonstrated that the size of the microcracks at the solid-ice interface is the critical parameter that governs ice adhesion to a hydrophobic solid, and in case of the provision of sufficiently large voids at the interface, some SHS would reduce ice adhesion.[170] According to the analysis of Michael and Vahid, the critical shear stress (τ_{yy}) correlates with the receding CA (θ_{rec}) and crack length (a), which obeys the equation 23:

$$\tau_{yy} = \sqrt{\frac{E G_{rec}}{\pi a}} = \sqrt{\frac{E \gamma_{IA}(1 + \cos\theta_{rec})}{\pi a}} \qquad (29)$$

Where E, G_{rec}, γ_{IA} are the Young modulus, the surface energy of the receding crack, and the ice-air interfacial energies, respectively. That's why some SHS have strong ice adhesion in case of no provision of sufficiently large voids at the interface. As for ice-phobic and hydrophobic, the water/ice repellency may be the apparent similarity, but apart from that, there are similarities on other levels including the phobic effect, interactions and mechanisms as shown in Figure 7C. Furthermore, Vahid et al. report how ice adhesion is different from water using force balance analysis, and why SHS are not necessary ice-phobic.[169] Through their theoretical force analysis, they reached that the contact angle hysteresis is the key parameter to affect droplet adhesion on surfaces, while for ice nucleation, both receding contact angle and the size of voids are the key parameters, but not always correlate with those, which depended on the definition of these phenomenon.

Actually, as for the ice-phobic of materials, wettability (contact angle, wetting hysteresis, or receding angle) and surface roughness (morphology) are combined to influence on the crystallization and nucleation, and further affect the ice adhesion through the combination effect.[176] Ice adhesion correlates with water contact angle only in case of similar roughness, and high surface roughness may lead a large ice adhesion.[177, 178] Wang et al. demonstrated that microstructure would result in a smaller ice adhesion on SHS, compared with the bare and hydrophobic surface. Due to the presence of large water contact angle and small water sliding angle, even under low temperature conditions, SHS with micro-nanoscale decreased the water/ice-solid contact fraction, which further leaded a low ice adhesion and durability of ice-phobic.[179] Furthermore, Bharathidasan et al. studied and evaluated the anti-icing properties of hydrophilic, hydrophobic and SHS, they concluded that smooth surface with low surface energy prefer to possess low ice-adhesion.[180]

3. The fabrication and further fundamental research of bionic anti-icing materials

Nowadays, research on anti-icing & ice-phobic coatings have mainly focused on two aspects, that is low-surface energy coatings and slippery liquid-infused layered coatings.[181] As for these two aspects, we will introduce them in more detail below.

3.1. Low-surface energy coatings

Previous research reveals that the ice adhesion of surface has correlations with surface wettability, including contact angle, wetting hysteresis, receding angle and

dynamic hydrophobicity.[166-168] Meanwhile, roughness of surface morphologies are combined to act on ice adhesion due to different ice-solid contact areas.[182] As for low-surface energy coatings, dip coating, vapor deposition, spray coating are three main strategies to fabricate coatings, and the ice adhesion on surfaces depend on four factors, that is hydrogen bonding, van der Waals forces and electrostatic interaction.[181]

3.1.1 Fluoride-containing polymer coatings

Among the fluoride-containing polymer coatings, Polytetrafluoroethylene (PTFE) are the common low surface energy of materials applied in metal and other metallic oxide, such as aluminum, iron, titanium, glass. Richard et al. fabricated an extremely adherent PTFE coating on an Al_2O_3 underlayer produced by anodizing in a phosphoric acid electrolyte, followed by an etching step. It was found that these coatings showed superhydrophobic properties and had the 20% ice adhesion value of bare aluminum. Moreover, it still stayed icephobicity at least for 14 surface smoothing tests.[183] Yang et al. investigated the ice-phobic performance of fluoropolymer materials, including pristine PTFE plates (P-PTFE), sandblasted PTFE plates (SB-PTFE), two PTFE coatings (SNF-1 and SNF-CO_1), a fluorinated room-temperature vulcanized silicone rubber coating (F-RTV) and a fluorinated polyurethane coating (F-PU), they found that the fluoropolymer material with a smooth surface can remarkably reduce ice adhesion strength, which is composite to the fluoropolymer material with sub-micron surfaces, especially at lower temperature and under higher humidity (**Figure 8A-B**).[184]

Via a unique solvent-free and substrate-independent method of initiated chemical vapor deposition (iCVD) for the creation of thin cross-linked bilayer films (Figure 8C),

Hossein et al. synthesized thin films of bilayer poly (divinyl benzene) p(DVB)/poly (perfluorodecylacrylate) (p-PFDA) on steel and silicon substrates. They found that the bilayer structure could enhance the elastic modulus and hardness of the films, and in situ grafting mechanism could improve the adhesion of the films to the substrate. Experiments revealed that these bilayer polymer networks could significantly reduce the strength of ice adhesion to the treated surfaces.[185] Via this method of iCVD, Yagüe and Gleason synthesized thin films of 1H,1H,2H,2H-perfluorodecyl acrylate copolymerized with the cross-linker divinylbenzene (p(PFDA-co-DVB)). They demonstrated that the cross-linking can provide a steric barrier to the reconstruction of the surface fluorinated groups when switching between dry and wet conditions and is a key factor for the reduction of CA hysteresis (Figure 8D).[186]

However, the production of these fluoropolymers may generate the pollution through the oxidative degradation, including perfluoroalkyl acid and perfluoroalkyl sulfonate, which has a potential environmental risk for healthy, therefore researchers should found the other fluorinated and nonfluorinated chemicals to replace long-chain perfluoroalkyl acids and their precursors. Aiming to develop a fluoropolymer design principle for high dynamic water repellency with short perfluoroalkyl side chains. Jiang et al. disclosed the effects of the α-substituent of the fluorinated acrylate, the spacer group, and the crystalline hydrocarbon pendant groups of the (co)polymer on the wettability performance and surface molecular rearrangement, which will bring more application in water-harvesting, self-cleaning, anti-icing and other fields.[187]

3.1.2 Silicon-containing polymer coatings

Polysilicon is another polymer coatings that can be applied in anti-icing materials.[152] Previous research reveals that fluoropolymer silicone coating has high adhesion compared with polysilicon.[188, 189] Using this kind of coatings, Liao et al. fabricated superhydrophobic ZnO film with nanorods on glass via RF magnetron sputtering, exhibiting an excellent anti-icing property in glaze ice, which is attributed to the nano-scale roughness and low surface energy of the as-prepared coating of hexadecyltrimethoxy silane (HDTMS).[190] Meanwhile, Wang et al. also prepared an excellent surface with the anti-icing properties based on the octadecyltrichlorosilane (OTS)-modified silica nanoparticles via a spray-coating process as shown in **Figure 9A**. Different from Liao et al., the glass performed a transparent property with exhibiting a transmittance above 81.5 % in the whole wavelength range of visible light. Furthermore, based on the performance of freezing delay time of droplets on the superhydrophobic coating surface at different temperature and wind velocities (Figure 9B), they proposed the icing and anti-icing mechanisms under wind action on surfaces with different wettabilities (Figure 9C).[191]

Wynne investigated the correlation between ice adhesion and coating thickness of polydimethylsiloxane (PDMS) elastomer (Sylgard 184). As shown in Figure 9D, results revealed that the peak removal shear force was decreased four times as the coating thickness ranging from 18 to 533 μm. The thickness act an important role in promoting large vertical displacement which guided to build up stress not only at the interface plane, but also at the frontier point or line.[192]

3.1.3 Fluorosilicone copolymer coatings

The effect of low surface energy resin combined with fluorine and silicon is better than single fluoride or silicon-based polymer. Via free radical polymerization of methyl methacrylate (**Figure 10A**), n-butyl acrylate and hydroxyethyl methacrylate using polymethyltrifluoropropylsiloxane macroazoinitiator (PMTFPS-MAI) in range of 10-50 wt%, Yuan et al. synthesized the fluorosilicone-containing block copolymers (PMTFPS–bpolyacrylate). They investigated that maximal delayed icing time and reduction of the ice shear strength occurred on sample P_2 with the 20 wt% content of PMTFPS-MAI, the ice shear strength was significantly lower than that of the polyacrylates as shown in Figure 10B. Experiments revealed that the delayed icing time was related to the surface roughness and enrichment of PMTFPS blocks on the copolymer surface; synergistic effect of silicone and fluorine could reduce the ice shear strength.[193] Thereby, as shown in Figure 10C, via hydrosilylation of polymethylhydrosiloxane (PMHS) with x fluorinated methacrylate (xFMA), they fabricated a series of fluorinated PMHS/octavinyl-polyhedral oligomeric silsesquioxanes (OVPOSS) hybrid films. Experiments suggested that the longer fluorinated side groups in PMHS–13FMA and PMHS–17FMA were conducive to strengthen its migration towards the film surface, and low solid–water interactions of their submicron/nano-structure, which were essential for the enhancement of hydrophobicity. As shown in Figure 10D, S13F with 10 wt% of OVPOSS prepared by PMHS–13FMA displayed the lowest ice shear strength among all the samples, which was related to the surface energy and surface roughness. Because of the higher interfacial interactions between film surfaces and ice/water, S17F possessed the higher

ice shear strengths, which benefit for opening insights into designing submicron/nano-structured polymer surface materials to have a better performance in practice.[194]

Fu et al. fabricated sol−gel coatings with different roughness and surface energy on glass substrates. They used Methyltriethoxysilane (MTEOS), 3-Glycidyloxypropyl trimethoxysilane (GLYMO) and fluoroalkylsilane (FAS) to obtain a mechanically robust ice-phobic coating. Experiments revealed that the intrinsic surface energy and surface morphology of the coatings act important roles together as shown in Figure E-G. Low surface roughness combined with the reduced surface energy leads to decreased ice adhesion compared with the uncoated bare glass. The addition of FAS effectively reduced the intrinsic surface energy of the coating and contributes to the superhydrophobicity at subzero temperatures, combined with the increasing surface roughness.[195]

However, the degradation product of fluorosilicone polymers, fluoropolymers has a bad effect on environment and causes a potentially harmful to human beings, therefore, the limited use of fluorosilicone polymers have been focused by more and more researchers. Green and environmental friendly coatings are encouraged to be instead of the fluorosilicone polymers.

3.2. Slippery liquid-infused layered coatings

Recently, liquid-infused layered coatings have been focused by most of researchers since Aizenberg et al. first created a slippery, ice-phobic surface on aluminum surfaces via a scalable and reproducible coating method. This slippery

liquid-infused porous surface (SLIPS)-coated surfaces not only significantly reduce ice accumulation by allowing the condensed water droplets to slide off before they freeze but also enable the easy removal of the accumulated ice and melted water by gravity at low tilt angles, and reduced ice adhesion strength of SLIPS significantly compared to conventional materials, which provides a great opportunity to utilize SLIPS-based ice-phobic surfaces for broad applications in the future.[196] Based on infused liquids, the liquid-infused SLIPS can be divided into the oil-infused SLIPS and aqueous-infused SLIPS.

3.2.1 Oil lubricating slippery surfaces

Hozumi et al. successfully fabricated self-lubricating organogels (SLUGs) by a simple crosslinking reaction of polydimethylsiloxanes (PDMS) in the presence of several organic liquids (**Figure 12A**). As shown in Figure 12C, the polymer main chain was attached with vinyl and Si−H groups to obtain a crosslinking capability, meanwhile to ensure a nonpolar chemical structure. Due to the syneresis of organogels, a liquid layer is continuously formed on the topmost SLUG surfaces under appropriate conditions, which resulted multi-liquid repellency, no matter including water-repellency and viscous emulsions-repellency but also ice-repellency which can be revealed from the Figure 12B.[197] Using the mechanism of this method (Figure 12A), Zhu et al. prepared silicon-oil-infused PDMS coatings with different silicon oil contents, which displays a low surface energy and low ice adhesion strength, only about 3% of the value on a bare aluminum surface. Owing to the low surface energy of the silicon oil and PDMS, and the high mobility of silicon oil, the surface showed a large water

contact angle and a small contact area, which leaded to the formation of a loose ice layer. Additionally, due to much contact of the ice with the mobile oil, the oil infused polymer structure significantly reduces the contact area of the ice with substrate, which leaded to a very weak interaction between the substrate and ice, and then markedly reduced the ice adhesion strength on the substrate, which could be a good idea for the fabrication of ice-phobic coatings.[198]

As shown in Figure 12D, Zhou et al. fabricated a photothermal ice-phobic film which possessed both the durable lubricating effect and the photothermal effect. From the idea of concept, it is ascribed to the presence of a liquid interface which is firmly locked in porous structures and forms a defect-free interface, so that it can significantly reduce the ice adhesion strength (Figure 12E). Additionally, Due to the addition of Fe_3O_4 nanoparticles, the film can afford high efficiency photothermal effect under near-infrared irradiation for rapidly melting, which inspired and instructed the design and fabrication of various next-generation anti/deicing materials.[199]Bioinspired from the nature creature, researchers have obtained abundant inspiration. Inspired by natural systems that secrete a functional liquid in response to stimuli, Rykaczewski et al. introduced an anti-icing coating that responds to surface icing by releasing antifreeze liquid as shown in Figure 12F. It included an outer epidermis with superhydrophobic pores and an underlying dermis with antifreeze infused wick. The functionality of the new coating is validated through condensation frosting, simulated freezing fog, and freezing rain experiments, and verified that the introduced anti-icing skin significantly delayed onset of frost, rime, and glaze accumulation compared with anti-icing

superhydrophobic and lubricant impregnated surfaces, which could be an inspiration for further bioinspired research on anti-icing & ice-phobic materials.[200]

3.2.2 Aqueous lubricating slippery surfaces

Another kind of liquid-infused layered coating is lubricating slippery surface. This anti-icing coating can be directly applied to various substrates, and the ice adhesion strength on the coated surfaces can be reduced more significantly than uncoated substrates.[201-206] Wang et al. fabricated a series of anti-icing coatings with aqueous lubricating slippery surfaces, including crosslinked poly(acrylic acid), hyaluronic acid and hydrophillic polyurethane particles.[201, 203, 204, 207] Via grafting cross-linked hygroscopic polymers inside the micropores at the surface of inorganic materials (**Figure 13A**), they fabricated a robust prototypical anti-icing coating with a self-lubricating liquid water layer (SLWL), where the accumulated ice could be blown off by an action of strong breeze. Experiments' results of the ice adhesion strength on varioous surfaces revealed that when the area fraction (ϕ) value is greater than 0.2 and the surface is SLWL, ice adhesion was lower than the other surfaces as shown in Figure B-C. Especially, the ice adhesion strength on surfaces with SLWL remained stable when the temperature was reduced till −25 °C (Figure 13D). Moreover, the SLWL surface exhibits excellent mechanical durability and capability of self-healing after 80 abrasion cycles as shown in Figure 13E.[201] Furthermore, they fabricated another anti-icing coating via the method of spincoating, mixing the PU, curing agent and γ-butyrolacone, and thermally curation as shown in **Figure 14A-B**. They also veryfied that that the ice nucleus on this coating could be blown off with a strong breeze action

in a wind tunnel, and stayed the robustness and of the anti-icing coating after icing/de-icing processes. Differently, the low ice adhesion of the anti-icing coating could be kept even when the temperature is reduced to -53 ℃ (Figure 14C-D), which bring a great promise for practical applications of anti-icing coating with an aqueous lubricating layer.[203] As for SLWL coating, they further fabricated anti-icing coating with an aqueous lubricating layer using the dopamine-modified hyaluronic acid, and found that the thickness of aqueous lubricating layer acted an important role in the anti-icing performance. In case of the aqueous lubricating layer thickness of 20 nm, ice adhesion strength was the best and more than one order of magnitude lower than that of uncoated metal or alumina ceramic surfaces, and less than half of that on the synthetic polymers. Importantly, their method could be applied to all types of solid surfaces due to the nonselective adhesive property of dopamine factly, which can provide a low-cost approach to fabricate the anti-ice coating in the future.[207]

On the other hand, ion polymers can be also applied in the fabrication of SLIPS. Chernyy et al. introduced a superhydrophilic polyelectrolyte brush (PB) coatings via ion exchange, incorporating mono-, bi-, and trivalent ions, which performed an excellent anti-icing properties. Experiments revealed that the strongest kosmotropes, Li+ and Na+, were able to reduce ice adhesion by 40% and 25%, respectively at −18 ℃, ascribing to hydration of ions, but no effect on ice adhesion for the weak kosmotropes and chaotropes.[202] Furthermore, due to the fact that ions at the PB/water interface can be reversibly exchanged, Wang et al. found that the effect of ions on heterogeneous ice

nucleation on the PB surface, and discovered that the distinct efficiency of ions in tuning HIN follows the Hofmeister series. [204]

4. Conclusion

Nowadays, ice accumulating causes various problems on solid surface, such as on roads, aircrafts, power lines, ships, and some energy equipment, which becomes a worldwide issue and affects our daily lives. Even though some traditional prevention methods could sove the problem of ice accumulation to some extent based on the thought of deicing or melting ice, they can't solve the problem fundamentally and produce large amounts of energy consumption, ascribing to thermal, mechanical and other passive de-icing methods. Therefore, Widespread attention has been attracted into the anti-icing & ice-phobic coatings, which is designed to suppress or delay the formation of ice nucleatione, reduce the ice adhesion, and lessen energy consumption on the material surfac. Excellent ice prevention coatings can not only reduce ice-adhesion, but also delay water freezing on surfaces, which avoid much ice accumulation on such coated surfaces.

In this review, we first outline the background of anti-icing & ice-phobic technology and its existing methods, including thermal de-icing, mechanical de-icing and other passive de-icing methods. In what follows, theory of anti-icing and theory of ice-phobic are introduced in detail, including the mechanism of condensate microdrops self-propelling, drops bouncing, wetting, ice nucleation and ice adhesion, respectively. Subsequently, we introduce recent development in research on the fabrication and

further fundamental research of biomimetic materials for anti-icing & ice-phobic. Special emphasis is placed on two parts, that is low-surface energy coatings and liquid-infused layered coatings with discussion on the recent progress and comparison. As for low-surface energy coatings, fluoride-containing polymer coatings, silicon-containing polymer coatings, and fluorosilicone copolymer coatings are compared with each other. As for liquid-infused layered coatings, oil lubricating slippery surfaces and aqueous lubricating slippery surfaces are compared with each other. Finally, based on exsisting technology in previous research, we draw conclusions for comparison and outlooks for future consideration of the anti-icing & ice-phobic technology.

Learning from the nature, we have obtained plenty of inspiration and prepared bioinspired anti-icing & ice-phobic materials. At present, the hot focus of the anti-icing coatings is the superhydrophobic hard surface, but there exists two obstacles, that are how to maintain the performance of superhydrophobic property under low temperature and high humidity environment, and how to ensure that structure will not be broken in an icing-deicing cycle. To obtain the functional surfaces intergrated with the property of anti-icing and ice-phobic, wettability and roughness are the primary factor to achieve this goal. As for superhydrophobic coatings, the roughness act a significant role in the enhanced hydrophobic property of nano-structure. So, regulating the roughness may enhace the anti-icing property as a key parameter for consideration. As for SLIPS coatings, grafting the hydrophilic group transforms the quantitative relation of the ice adhesion with the microstructure through wettability optimization, which further improves the ice-phobic property of SLIPS coatings. But besides conventional hard

substrates, soft materials with low thermal conductivity should be paid more attention. Attributing to the integrated effect of the composite flexibility and the hierarchical structure (micro/nano-structure), flexible-superhydrophobic surfaces (FS-surfaces) usually show an excellent water and ice repellency at low temperatures under high relatively humidity condition for a long time. Therefore, as for soft materials, micro and nanostructures are the key reason for the stability of the structure and its excellent long-term water/ice repellency.[208]

Whereas, researches on anti-icing & ice-phobic coatings still remain in the stage of laboratory. Meanwhile, there is no uniform standard of test methods. Freezing temperature, freezing time, nucleation rate, and ice adhesion are also used as measure against the anti-icing & ice-phobic effect factors, but using no commonly used test methods. Additionally, the natural environment is relatively complex and affects more factors, such as wind speed, the angle of cold droplet impact, and the adhesion of pollutants. Some potential issues about anti-icing & ice-phobic technology should be noted, such as high cost, strong dependence of equipment research. Importantly, heat transferring on supperwetting surfaces are rarely analysized in the research of anti-icing & icephobic. Researches revealed that some specific nanosample exhibited over 100% enhancement in dropwise condensate heat transfer coefficient, which provide a new approach to characterize the ability of anti-icing & ice-phobic.[209, 210] As a result, there is still a long way to go before the anti-icing & ice-phobic coatings are industrialized.

Allowing for the requirements of environment-friendly, easy realization of industrialization, the stability and durability of anti-icing & ice-phobic coatings, smart

multi-functional anti-icing & ice-phobic surface will become an important research direction, such as temperature sensitive polymer ─ poly(N-isopropyl acrylamide) (PNIPAAm), can change the volume and surface morphology reversibly with the temperature changing, which is ascribed to conformational change of the polymer chains reversibly.[211] Even though the temperature range of conformational change is far above the freezing point of water, it can be expected that smart surfaces sensitive to the temperature or other conditions would be finally developed for anti-icing & ice-phobic in the future.

Acknowledgements

The authors thank the National Natural Science Foundation of China (21501127; 51502185), Natural Science Foundation of Jiangsu Province of China (BK20140400). We also acknowledge the funds from the project of the Priority Academic Program Development of Jiangsu Higher Education Institutions (PAPD), Natural Science Foundation of the Jiangsu Higher Education Institutions of China (15KJB430025), and Project for Jiangsu development and innovation of graduate students (2017).

Received: ((will be filled in by the editorial staff))
Revised: ((will be filled in by the editorial staff))
Published online: ((will be filled in by the editorial staff))

References:

[1] D. Aydın, R. Kizilel, R. O. Caniaz, S. Kizilel, *Ind Eng. Chem. Res.* **2015**, *54*, 12587.

[2] Z. Chunxiu, T. Yiqiu, *Road Mater. Pavement* **2011**, *10*, 281.

[3] E. Cuelho, J. Harwood, *Transport. Res. Rec.* **2012**, *2272*, 144.

[4] L. Fu, R. Omer, C. Jiang, *Transport. Res. Rec.* **2012**, *2272*, 130.

[5] F. Giuliani, F. Merusi, G. Polacco, S. Filippi, M. Paci, *Constr. Build. Mater.* **2012**, *30*, 174.

[6] E. Heymsfield, A. Osweiler, P. Selvam, M. Kuss, *J. Cold Reg. Eng.* **2014**, *28*, 04014001.

[7] S. M. K. Hossain, L. Fu, A. J. Olesen, *Can. J. Civil Eng.* **2014**, *41*, 523.

[8] A. Klein-Paste, J. Wåhlin, *Cold Reg. Sci. Technol.* **2013**, *96*, 1.

[9] X. Shi, K. Fortune, L. Fay, R. Smithlin, D. Cross, Z. Yang, J. Wu, *Cold Reg. Sci. Technol.* **2012**, *83-84*, 89.

[10] H. Wei, Q. He, Y. Jiao, J. Chen, M. Hu, *Constr. Build. Mater.* **2016**, *107*, 109.

[11] O. Xu, S. Han, C. Zhang, Y. Liu, F. Xiao, J. Xu, *Constr. Build. Mater.* **2015**, *98*, 671.

[12] L. M. Young, S. A. Durham, *J. Perform. Constr. Fac.* **2013**, *27*, 836.

[13] M. Zheng, J. Zhou, S. Wu, H. Yuan, J. Meng, *Constr. Build. Mater.* **2015**, *84*, 277.

[14] A. P. Broeren, S. Lee, C. Clark, *J. Aircraft* **2016**, *53*, 451.

[15] J. M. Brown, S. Raghunathan, J. K. Watterson, A. J. Linton, D. Riordon, *J. Aircraft* **2002**, *39*, 65.

[16] M. P. C. Pellissier, W. G. Habashi, A. Pueyo, *J. Aircraft* **2011**, *48*, 265.

[17] W. Dong, J. Zhu, M. Zheng, G. L. Lei, Z. X. Zhou, *J. Propul. Power* **2015**, *31*, 1330.

[18] R. Hannat, J. Weiss, F. Garnier, F. Morency, *Eng. Appl. Comp. Fluid* **2015**, *8*, 530.

[19] O. Harireche, P. Verdin, C. P. Thompson, D. W. Hammond, *J. Aircraft* **2008**, *45*, 1924.

[20] J. La Due, M. R. Muller, M. Swangler, *J. Aircraft* **1996**, *33*, 131.

[21] M. Mohseni, A. Amirfazli, *Cold Reg. Sci. Technol.* **2013**, *87*, 47.

[22] S. Özgen, M. Carbonaro, G. S. R. Sarma, *Phys. Fluids* **2002**, *14*, 3391.

[23] O. Parent, A. Ilinca, *Cold Reg. Sci. Technol.* **2011**, *65*, 88.

[24] M. Pourbagian, W. G. Habashi, *J. Aircraft* **2013**, *50*, 1555.

[25] M. Pourbagian, B. Talgorn, W. G. Habashi, M. Kokkolaras, S. Le Digabel, *Optim. Eng.* **2015**, *16*, 663.

[26] S. K. Thomas, R. P. Cassoni, C. D. MacArthur, *J. Aircraft* **1996**, *33*, 841.

[27] J. Zhu, W. Dong, M. Zheng, G. Lei, Q. Zhao, *J. Propul. Power* **2016**, *32*, 789.

[28] C. Zilio, L. Patricelli, *Appl. Therm. Eng.* **2014**, *63*, 40.

[29] X. Wei, Z. Jia, Z. Sun, M. Farzaneh, Z. Guan, *IEEE T. Power Deliver.* **2016**, *31*, 1413.

[30] X. Wei, Z. Jia, Z. Sun, Z. Guan, M. MacAlpine, *IEEE Electr. Insul. M.* **2014**, 42.

[31] X. Wei, Z. Jia, Z. Sun, W. Liao, Y. Qin, Z. Guan, *IEEE T. Dielect. El. In.* **2012**, *19*, 2063.

[32] Z. Xu, Z. Jia, Z. Li, X. Wei, Z. Guan, M. MacAlpine, *IEEE T. Dielect. El. In.* **2011**, *18*, 760.

[33] J. Lv, Y. Song, L. Jiang, J. Wang, *ACS Nano* **2014**, *8*, 3152.

[34] W. Barthlott, C. Neinhuis, *Planta* **1997**, *202*, 1.

[35] E. P. Ivanova, J. Hasan, H. K. Webb, V. K. Truong, G. S. Watson, J. A. Watson, V. A. Baulin, S. Pogodin, J. Y. Wang, M. J. Tobin, C. Lobbe, R. J. Crawford, *Small* **2012**, *8*, 2489.

[36] X. Gao, X. Yan, X. Yao, L. Xu, K. Zhang, J. Zhang, B. Yang, L. Jiang, *Advanced Materials* **2007**, *19*, 2213.

[37] H. Chen, P. Zhang, L. Zhang, H. Liu, Y. Jiang, D. Zhang, Z. Han, L. Jiang, *Nature* **2016**, *532*, 85.

[38] Y. Zheng, X. Gao, L. Jiang, *Soft Matter* **2007**, *3*, 178.

[39] S. G. Lee, H. S. Lim, D. Y. Lee, D. Kwak, K. Cho, *Advanced Functional Materials* **2013**, *23*, 547.

[40] Y. Lai, J. Huang, Z. Cui, M. Ge, K. Q. Zhang, Z. Chen, L. Chi, *Small* **2016**, *12*, 2203.

[41] S. Zhang, J. Huang, Z. Chen, Y. Lai, *Small* **2017**, *13*, 1602992.

[42] S. Li, J. Huang, Z. Chen, G. Chen, Y. Lai, *J. Mater. Chem. A* **2017**, *5*, 31.

[43] C. Cao, M. Ge, J. Huang, S. Li, S. Deng, S. Zhang, Z. Chen, K. Zhang, S. S. Al-Deyab, Y. Lai, *J. Mater. Chem. A* **2016**, *4*, 12179.

[44] J. Y. Huang, Y. K. Lai, F. Pan, L. Yang, H. Wang, K. Q. Zhang, H. Fuchs, L. F. Chi, *Small* **2014**, *10*, 4865.

[45] Y. Lai, L. Lin, F. Pan, J. Huang, R. Song, Y. Huang, C. Lin, H. Fuchs, L. Chi, *Small* **2013**, *9*, 2945.

[46] Y. Lai, F. Pan, C. Xu, H. Fuchs, L. Chi, *Adv. Mater.* **2013**, *25*, 1682.

[47] Y. Lai, Y. Tang, J. Gong, D. Gong, L. Chi, C. Lin, Z. Chen, *J. Mater. Chem.* **2012**, *22*, 7420.

[48] J. Mao, M. Ge, J. Huang, Y. Lai, C. Lin, K. Zhang, K. Meng, Y. Tang, *J. Mater. Chem. A* **2017**, *5*, 11873.

[49] Q. Wang, X. Yao, H. Liu, D. Quere, L. Jiang, *Proc. Natl. Acad. Sci. USA* **2015**, *112*, 9247.

[50] K. M. Wisdom, J. A. Watson, X. Qu, F. Liu, G. S. Watson, C. H. Chen, *Proc. Natl. Acad. Sci. USA* **2013**, *110*, 7992.

[51] R. Enright, N. Miljkovic, A. Al-Obeidi, C. V. Thompson, E. N. Wang, *Langmuir* **2012**, *28*, 14424.

[52] R. Enright, N. Miljkovic, J. L. Alvarado, K. Kim, J. W. Rose, *Nanosc. Microsc. Therm.* **2014**, *18*, 223.

[53] B. S. Sikarwar, S. Khandekar, S. Agrawal, S. Kumar, K. Muralidhar, *Heat Transfer Eng.* **2012**, *33*, 301.

[54] J. B. Boreyko, C. H. Chen, *Phys. Rev. Lett.* **2009**, *103*, 184501.

[55] J. Feng, Z. Qin, S. Yao, *Langmuir* **2012**, *28*, 6067.

[56] Y. Lai, X. Gao, H. Zhuang, J. Huang, C. Lin, L. Jiang, *Adv. Mater.* **2009**, *21*, 3799.

[57] R. Raj, R. Enright, Y. Zhu, S. Adera, E. N. Wang, *Langmuir* **2012**, *28*, 15777.

[58] W. Choi, A. Tuteja, J. M. Mabry, R. E. Cohen, G. H. McKinley, *J. Colloid Interf. Sci.* **2009**, *339*, 208.

[59] W. Li, A. Amirfazli, *J. Colloid Interf. Sci.* **2005**, *292*, 195.

[60] S. Zhang, J. Huang, Y. Tang, S. Li, M. Ge, Z. Chen, K. Zhang, Y. Lai, *Small* **2017**, *13*, 1600687.

[61] J. Tian, J. Zhu, H. Y. Guo, J. Li, X. Q. Feng, X. Gao, *J. Phys. Chem. Lett.* **2014**, *5*, 2084.

[62] R. Enright, N. Miljkovic, J. Sprittles, K. Nolan, R. Mitchell, E. N. Wang, *ACS Nano* **2014**, *8*, 10352.

[63] X. Liu, P. Cheng, X. Quan, *Int. J. Heat Mass Tran.* **2014**, *73*, 195.

[64] F. Liu, G. Ghigliotti, J. J. Feng, C.-H. Chen, *J. Fluid Mech.* **2014**, *752*, 39.

[65] F.-C. Wang, F. Yang, Y.-P. Zhao, *Appl. Phys. Lett.* **2011**, *98*, 053112.

[66] Y. Nam, H. Kim, S. Shin, *Appl. Phys. Lett.* **2013**, *103*, 161601.

[67] W. Zhang, G. Lin, J. Li, H. Xue, Y. Luo, X. Gao, *Adv. Mater. Interfaces* **2015**, *2*, 1500238.

[68] Y. Cho, G. Kim, Y. Cho, S. Y. Lee, H. Minsky, K. T. Turner, D. S. Gianola, S. Yang, *Adv. Mater.* **2015**, *27*, 7788.

[69] J. Li, W. Zhang, Y. Luo, J. Zhu, X. Gao, *ACS Appl. Mater. Interfaces* **2015**, *7*, 18206.

[70] J. Liu, H. Guo, B. Zhang, S. Qiao, M. Shao, X. Zhang, X. Q. Feng, Q. Li, Y. Song, L. Jiang, J. Wang, *Angew. Chem. Int. Edit.* **2016**, *55*, 4265.

[71] Y. Luo, J. Li, J. Zhu, Y. Zhao, X. Gao, *Angew. Chem. Int. Edit.* **2015**, *54*, 4876.

[72] B. Mondal, M. Mac Giolla Eain, Q. Xu, V. M. Egan, J. Punch, A. M. Lyons, *ACS Appl. Mater. Inter.* **2015**, *7*, 23575.

[73] J. Tian, Y. Zhang, J. Zhu, Z. Yang, X. Gao, *Chemphyschem* **2014**, *15*, 858.

[74] Y. Zhao, Y. Luo, J. Li, F. Yin, J. Zhu, X. Gao, *ACS Appl. Mater. Inter.* **2015**, *7*, 11079.

[75] X. Jin, X. Zhang, Y. Peng, M. Cao, H. Liu, X. Pei, K. Liu, L. Jiang, *Adv. Eng. Mater.* **2015**, *17*, 961.

[76] J. Li, Y. Luo, J. Zhu, H. Li, X. Gao, *ACS Appl. Mater. Inter.* **2015**, *7*, 26391.

[77] N. Miljkovic, R. Enright, Y. Nam, K. Lopez, N. Dou, J. Sack, E. N. Wang, *Nano Lett.* **2013**, *13*, 179.

[78] R. D. Narhe, M. D. Khandkar, P. B. Shelke, A. V. Limaye, D. A. Beysens, *Phys. Rev. E* **2009**, *80*, 031604.

[79] Y. Cho, T. S. Shim, S. Yang, *Adv. Mater.* **2016**, *28*, 1433.

[80] M. He, Q. Zhang, X. Zeng, D. Cui, J. Chen, H. Li, J. Wang, Y. Song, *Adv. Mater.* **2013**, *25*, 2291.

[81] M. He, X. Zhou, X. Zeng, D. Cui, Q. Zhang, J. Chen, H. Li, J. Wang, Z. Cao, Y. Song, L. Jiang, *Soft Matter* **2012**, *8*, 6680.

[82] C. Lv, P. Hao, Z. Yao, Y. Song, X. Zhang, F. He, *Appl. Phys. Lett.* **2013**, *103*, 021601.

[83] N. Miljkovic, R. Enright, E. N.Wang, *ACS Nano* **2012**, *6*, 1776.

[84] J. B. Boreyko, C. P. Collier, *ACS Nano* **2013**, *7*, 1618.

[85] X. Chen, R. Ma, H. Zhou, X. Zhou, L. Che, S. Yao, Z. Wang, *Sci. Rep.* **2013**, *3*, 2515.

[86] X. Chen, J. Wu, R. Ma, M. Hua, N. Koratkar, S. Yao, Z. Wang, *Adv. Funct. Mater.* **2011**, *21*, 4617.

[87] J. Guadarrama-Cetina, A. Mongruel, W. González-Viñas, D. Beysens, *Europhys. Lett.* **2013**, *101*, 16009.

[88] Q. Zhang, M. He, J. Chen, J. Wang, Y. Song, L. Jiang, *Chem. Commun.* **2013**, *49*, 4516.

[89] Q. Zhang, M. He, X. Zeng, K. Li, D. Cui, J. Chen, J. Wang, Y. Song, L. Jiang, *Soft Matter* **2012**, *8*, 8285.

[90] L. Mishchenko, B. Hatton, J. Aizenberg, V. Bahadur, J. A. Taylor, T. Krupenkin, *ACS Nano* **2010**, *4*, 7699.

[91] T. Maitra, C. Antonini, M. K. Tiwari, A. Mularczyk, Z. Imeri, P. Schoch, D. Poulikakos, *Langmuir* **2014**, *30*, 10855.

[92] T. Maitra, M. K. Tiwari, C. Antonini, P. Schoch, S. Jung, P. Eberle, D. Poulikakos, *Nano Lett.* **2014**, *14*, 172.

[93] P. Tourkine, M. Le Merrer, D. Quere, *Langmuir* **2009**, *25*, 7214.

[94] J. C. Bird, R. Dhiman, H. M. Kwon, K. K. Varanasi, *Nature* **2013**, *503*, 385.

[95] A.-L. Biance, F. Chevy, C. Clanet, G. Lagubeau, D. Quéré, *J. Fluid Mech.* **2006**, *554*, 47.

[96] J. E. Field, *Wear* **1999**, *233-235*, 1.

[97] C. Hao, Y. Liu, X. Chen, J. Li, M. Zhang, Y. Zhao, Z. Wang, *Small* **2016**, *12*, 1825.

[98] C. Josserand, S. T. Thoroddsen, *Annu. Rev. Fluid Mech.* **2016**, *48*, 365.

[99] R. Rioboo, C. Tropea, M. Marengo, *Atomization Spray.* **2001**, *11*, 12.

[100] T. Tran, H. J. Staat, A. Prosperetti, C. Sun, D. Lohse, *Phys. Rev. Lett.* **2012**, *108*, 036101.

[101] L. Xu, W. W. Zhang, S. R. Nagel, *Phys. Rev. Lett.* **2005**, *94*, 184505.

[102] A. L. Yarin, *Annu. Rev. Fluid Mech.* **2006**, *38*, 159.

[103] S. Schiaffino, A. A. Sonin, *Phys. Fluids* **1997**, *9*, 3172.

[104] X. Deng, F. Schellenberger, P. Papadopoulos, D. Vollmer, H. J. Butt, *Langmuir* **2013**, *29*, 7847.

[105] D. B. van Dam, C. Le Clerc, *Phys. Fluids* **2004**, *16*, 3403.

[106] D. Richard, D. Quéré, *Europhys. Lett.* **2000**, *50*, 769.

[107] I. S. Bayer, C. M. Megaridis, *J. Fluid Mech.* **2006**, *558*, 415.

[108] C. Clanet, C. BéGuin, D. Richard, D. Quéré, *J. Fluid Mech.* **2004**, *517*, 199.

[109] J. de Ruiter, R. Lagraauw, D. van den Ende, F. Mugele, *Nat. Phys.* **2014**, *11*, 48.

[110] A. Mongruel, V. Daru, F. Feuillebois, S. Tabakova, *Phys. Fluids* **2009**, *21*, 032101.

[111] R. D. Schroll, C. Josserand, S. Zaleski, W. W. Zhang, *Phys. Rev. Lett.* **2010**, *104*, 034504.

[112] C. W. Visser, Y. Tagawa, C. Sun, D. Lohse, *Soft Matter* **2012**, *8*, 10732.

[113] S. Chandra, C. T. Avedisian, *Proc. R. Soc. Lond. A* **1991**, *432*, 13.

[114] M. Rein, *Fluid Dynamics Research* **1993**, *12*, 61.

[115] D. Richard, C. Clanet, D. Quéré, *Nature* **2002**, *417*, 811.

[116] M. Pasandideh‐Fard, Y. M. Qiao, S. Chandra, J. Mostaghimi, *Phys. Fluids* **1996**, *8*, 650.

[117] K. Okumura, F. Chevy, D. Richard, D.Quéré, C. Clanet, *Europhys. Lett.* **2003**, *62*, 237.

[118] D. Bartolo, C. Josserand, D. Bonn, *J. Fluid Mech.* **2005**, *545*, 329.

[119] F. E. C. Culick, *J. Appl. Phys.* **1960**, *31*, 1128.

[120] G. Taylor, *Proc. R. Soc. Lond. A* **1959**, *253*, 313.

[121] X. Li, X. Ma, Z. Lan, *Langmuir* **2010**, *26*, 4831.

[122] Y. Shen, J. Tao, H. Tao, S. Chen, L. Pan, T. Wang, *ACS Appl. Mater. Inter.* **2015**, *7*, 20972.

[123] A. Gauthier, S. Symon, C. Clanet, D. Quere, *Nat. Commun.* **2015**, *6*, 8001.

[124] Y. Shen, J. Tao, H. Tao, S. Chen, L. Pan, T. Wang, *Appl. Phys. Lett.* **2015**, *107*, 111604.

[125] Y. Liu, L. Moevius, X. Xu, T. Qian, J. M. Yeomans, Z. Wang, *Nat. Phys.* **2014**, *10*, 515.

[126] Y. Liu, M. Andrew, J. Li, J. M. Yeomans, Z. Wang, *Nat. Commun.* **2015**, *6*, 10034.

[127] D. Bartolo, F. Bouamrirene, É. Verneuil, A. Buguin, P. Silberzan, S. Moulinet, *Europhys. Lett.* **2006**, *74*, 299.

[128] S. Dash, M. T. Alt, S. V. Garimella, *Langmuir* **2012**, *28*, 9606.

[129] T. Deng, K. K. Varanasi, M. Hsu, N. Bhate, C. Keimel, J. Stein, M. Blohm, *Appl. Phys. Lett.* **2009**, *94*, 133109.

[130] D. Hee Kwon, S. Joon Lee, *Appl. Phys. Lett.* **2012**, *100*, 171601.

[131] J. Hyväluoma, J. Timonen, *Europhys. Lett.* **2008**, *83*, 64002.

[132] Y. C. Jung, B. Bhushan, *Langmuir* **2008**, *24*, 6262.

[133] A. Lafuma, D. Quéré, *Nat. Mater.* **2003**, *2*, 457.

[134] M. Reyssat, A. Pépin, F. Marty, Y. Chen, D. Quéré, *Europhys. Lett.* **2006**, *74*, 306.

[135] M. Reyssat, D. Richard, C. Clanet, D. Quéré, *Faraday Discussions* **2010**, *146*, 19.

[136] Z. Wang, C. Lopez, A. Hirsa, N. Koratkar, *Appl. Phys. Lett.* **2007**, *91*, 023105.

[137] H. M. Kwon, A. T. Paxson, K. K. Varanasi, N. A. Patankar, *Phys. Rev. Lett.* **2011**, *106*, 036102.

[138] M. K. Chaudhury, G. M. Whitesides, *Science* **1992**, *256*, 1539.

[139] K. H. Chu, R. Xiao, E. N. Wang, *Nat. Mater.* **2010**, *9*, 413.

[140] B. A. Malouin, N. A. Koratkar, A. H. Hirsa, Z. Wang, *Appl. Phys. Lett.* **2010**, *96*, 234103.

[141] M. Reyssat, F. Pardo, D. Quéré, *Europhys. Lett.* **2009**, *87*, 36003.

[142] J. Wu, R. Ma, Z. Wang, S. Yao, *Appl. Phys. Lett.* **2011**, *98*, 204104.

[143] T. Young, *Phil. Trans. R. Soc. Lond.* **1805**, *95*, 65.

[144] R. N. Wenzel, *Ind. Eng. Chem.* **1936**, *28*, 988.

[145] R. N. Wenzel, *J. Phys. Colloid Chem.* **1949**, *53*, 1466.

[146] A. B. D. Cassie, S. Baxter, *Trans. Faraday Soc.* **1944**, *40*, 546.

[147] C. G. L. Furmidge, *J. Colloid Sci.* **1962**, *17*, 309.

[148] S. Jung, M. K. Tiwari, N. V. Doan, D. Poulikakos, *Nat. Commun.* **2012**, *3*, 615.

[149] A. Alizadeh, M. Yamada, R. Li, W. Shang, S. Otta, S. Zhong, L. Ge, A. Dhinojwala, K. R. Conway, V. Bahadur, A. J. Vinciquerra, B. Stephens, M. L. Blohm, *Langmuir* **2012**, *28*, 3180.

[150] Q. T. Fu, E. J. Liu, P. Wilson, Z. Chen, *Phys. Chem. Chem. Phys.***2015**, *17*, 21492.

[151] P. Guo, Y. Zheng, M. Wen, C. Song, Y. Lin, L. Jiang, *Adv. Mater.* **2012**, *24*, 2642.

[152] L. Cao, A. K. Jones, V. K. Sikka, J. Wu, D. Gao, *Langmuir* **2009**, *25*, 12444.

[153] L. Yin, Q. Xia, J. Xue, S. Yang, Q. Wang, Q. Chen, *Appl. Surf. Sci.* **2010**, *256*, 6764.

[154] S. Jung, M. K. Tiwari, D. Poulikakos, *Proc. Natl. Acad. Sci. USA* **2012**, *109*, 16073.

[155] J. B. Boreyko, B. R. Srijanto, T. D. Nguyen, C. Vega, M. Fuentes-Cabrera, C. P. Collier, *Langmuir* **2013**, *29*, 9516.

[156] K. Li, S. Xu, W. Shi, M. He, H. Li, S. Li, X. Zhou, J. Wang, Y. Song, *Langmuir* **2012**, *28*, 10749.

[157] K. Li, S. Xu, J. Chen, Q. Zhang, Y. Zhang, D. Cui, X. Zhou, J. Wang, Y. Song, *Appl. Phys. Lett.* **2014**, *104*, 101605.

[158] G. R. Wood, A. G. Walton, *J. Appl. Phys.* **1970**, *41*, 3027.

[159] T. Inada, T. Koyama, F. Goto, T. Seto, *J. Phys. Chem. B* **2011**, *115*, 7914.

[160] R. W. Michelmore, F. Franks, *Cryobiology* **1982**, *19*, 163.

[161] D. Turnbull, B. Vonnegut, *Ind. Eng. Chem.* **1952**, *44*, 1292.

[162] K. K. Varanasi, T. Deng, J. D. Smith, M. Hsu, N. Bhate, *Appl. Phys. Lett.* **2010**, *97*, 234102.

[163] D. K. Sarkar, M. Farzaneh, *J. Adhes. Sci. Technol.* **2009**, *23*, 1215.

[164] H. H. G. JeUinek, *J. Colloid Sci.* **1959**, *14*, 268.

[165] S. A. Kulinich, M. Farzaneh, *Appl. Surf. Sci.* **2009**, *255*, 8153.

[166] A. Dotan, H. Dodiuk, C. Laforte, S. Kenig, *J. Adhes. Sci. Technol.* **2009**, *23*, 1907.

[167] S. A. Kulinich, M. Farzaneh, *Langmuir* **2009**, *25*, 8854.

[168] A. J. Meuler, J. D. Smith, K. K. Varanasi, J. M. Mabry, G. H. McKinley, R. E. Cohen, *ACS Appl. Mater. Inter.* **2010**, *2*, 3100.

[169] Y. Wang, J. Xue, Q. Wang, Q. Chen, J. Ding, *ACS Appl. Mater. Inter.* **2013**, *5*, 3370.

[170] M. Nosonovsky, V. Hejazi, *ACS Nano* **2012**, *6*, 8488.

[171] J. Chen, J. Liu, M. He, K. Li, D. Cui, Q. Zhang, X. Zeng, Y. Zhang, J. Wang, Y. Song, *Appl. Phys. Lett.* **2012**, *101*, 111603.

[172] S. A. Kulinich, S. Farhadi, K. Nose, X. W. Du, *Langmuir* **2011**, *27*, 25.

[173] V. Hejazi, K. Sobolev, M. Nosonovsky, *Sci. Rep.* **2013**, *3*, 2194.

[174] S. Farhadi, M. Farzaneh, S. A. Kulinich, *Appl. Surf. Sci.* **2011**, *257*, 6264.

[175] E. J. Ling, V. Uong, J. S. Renault-Crispo, A. M. Kietzig, P. Servio, *ACS Appl. Mater. Inter.* **2016**, *8*, 8789.

[176] S. Jung, M. Dorrestijn, D. Raps, A. Das, C. M. Megaridis, D. Poulikakos, *Langmuir* **2011**, *27*, 3059.

[177] M. Zou, S. Beckford, R. Wei, C. Ellis, G. Hatton, M. A. Miller, *Appl. Surf. Sci.* **2011**, *257*, 3786.

[178] M. Susoff, K. Siegmann, C. Pfaffenroth, M. Hirayama, *Appl. Surf. Sci.* **2013**, *282*, 870.

[179] F. Wang, F. Lv, Y. Liu, C. Li, Y. Lv, *J. Adhes. Sci. Technol.* **2013**, *27*, 58.

[180] T. Bharathidasan, S. V. Kumar, M. S. Bobji, R. P. S. Chakradhar, B. J. Basu, *Appl. Surf. Sci.* **2014**, *314*, 241.

[181] B. Liu, K. Zhang, C. Tao, Y. Zhao, X. Li, K. Zhu, X. Yuan, *RSC Adv.* **2016**, *6*, 70251.

[182] A. J. Meuler, G. H. Mckinley, R. E. Cohen, *ACS Nano* **2010**, *4*, 7048.

[183] R. Menini, Z. Ghalmi, M. Farzaneh, *Cold Reg. Sci. Technol.* **2011**, *65*, 65.

[184] S. Yang, Q. Xia, L. Zhu, J. Xue, Q. Wang, Q.-m. Chen, *Appl. Surf. Sci.* **2011**, *257*, 4956.

[185] H. Sojoudi, G. H. McKinley, K. K. Gleason, *Mater. Horiz.* **2015**, *2*, 91.

[186] J. L. Yagüe, K. K. Gleason, *Macromolecules* **2013**, *46*, 6548.

[187] J. Jiang, G. Zhang, Q. Wang, Q. Zhang, X. Zhan, F. Chen, *ACS Appl. Mater. Inter.* **2016**, *8*, 10513.

[188] H. Murasea, T. Fujibayashib, *Prog. Org. Coat.* **1997**, *31*, 97.

[189] H. Murase, K. Nanishi, H. Kocure, T. Fujibayashi, K. Tamura, N. Haruta, *Appl. Polym. Sci.* **1994** *54*, 2051.

[190] R. Liao, Z. Zuo, C. Guo, A. Zhuang, X. Zhao, Y. Yuan, *Appl. Surf. Sci.* **2015**, *356*, 539.

[191] F. Wang, S. Yu, J. Ou, W. Li, *J. Sol-Gel Sci. Techn.* **2015**, *75*, 625.

[192] C. Wang, T. Fuller, W. Zhang, K. J. Wynne, *Langmuir* **2014**, *30*, 12819.

[193] X. Li, Y. Zhao, H. Li, X. Yuan, *Appl. Surf. Sci.* **2014**, *316*, 222.

[194] Y. Li, C. Luo, X. Li, K. Zhang, Y. Zhao, K. Zhu, X. Yuan, *Appl. Surf. Sci.* **2016**, *360*, 113.

[195] Q. Fu, X. Wu, D. Kumar, J. W. Ho, P. D. Kanhere, N. Srikanth, E. Liu, P. Wilson, Z. Chen, *ACS Appl. Mater. Inter.* **2014**, *6*, 20685.

[196] P. Kim, T.-S. Wong, J. Alvarenga, M. J. Kreder, W. E. Adorno-Martinez, J. Aizenberg, *ACS Nano* **2012**, *6*, 6569.

[197] C. Urata, G. J. Dunderdale, M. W. England, A. Hozumi, *J. Mater. Chem. A* **2015**, *3*, 12626.

[198] L. Zhu, J. Xue, Y. Wang, Q. Chen, J. Ding, Q. Wang, *ACS Appl. Mater. Inter.* **2013**, *5*, 4053.

[199] X. Yin, Y. Zhang, D. Wang, Z. Liu, Y. Liu, X. Pei, B. Yu, F. Zhou, *Adv. Funct. Mater.* **2015**, *25*, 4237.

[200] X. Sun, V. G. Damle, S. Liu, K. Rykaczewski, *Adv. Mater. Interfaces* **2015**, *2*, 1400479.

[201] J. Chen, R. Dou, D. Cui, Q. Zhang, Y. Zhang, F. Xu, X. Zhou, J. Wang, Y. Song, L. Jiang, *ACS Appl. Mater. Inter.* **2013**, *5*, 4026.

[202] S. Chernyy, M. Jarn, K. Shimizu, A. Swerin, S. U. Pedersen, K. Daasbjerg, L. Makkonen, P. Claesson, J. Iruthayaraj, *ACS Appl. Mater. Inter.* **2014**, *6*, 6487.

[203] R. Dou, J. Chen, Y. Zhang, X. Wang, D. Cui, Y. Song, L. Jiang, J. Wang, *ACS Appl. Mater. Inter.* **2014**, *6*, 6998.

[204] Z. He, W. J. Xie, Z. Liu, G. Liu, Z. Wang, Y. Q. Gao, J. Wang, *Sci. Adv.* **2016**, *2*, e1600345.

[205] Z. H. Ping, Q. T. Nguyen, S. M. Chen, J. Q. Zhou, Y. D. Ding, *Polymer* **2001**, *42*, 8461.

[206] R. Tadmor, N. Chen, J. N. Israelachvili, *J. Biomed. Mater. Res.* **2002**, *61*, 514.

[207] J. Chen, Z. Luo, Q. Fan, J. Lv, J. Wang, *Small* **2014**, *10*, 4693.

[208] L. Wang, Q. Gong, S. Zhan, L. Jiang, Y. Zheng, *Adv. Mater.* **2016**, *28*, 7729.

[209] Y. Zhao, Y. Luo, J. Zhu, J. Li, X. Gao, *ACS Appl. Mater. Inter.* **2015**, *7*, 11719.

[210] J. Zhu, Y. Luo, J. Tian, J. Li, X. Gao, *ACS Appl. Mater. Inter.* **2015**, *7*, 10660.

[211] H. Yang, H. Zhu, M. M. Hendrix, N. J. Lousberg, G. de With, A. C. Esteves, J. H. Xin, *Adv. Mater.* **2013**, *25*, 1150.

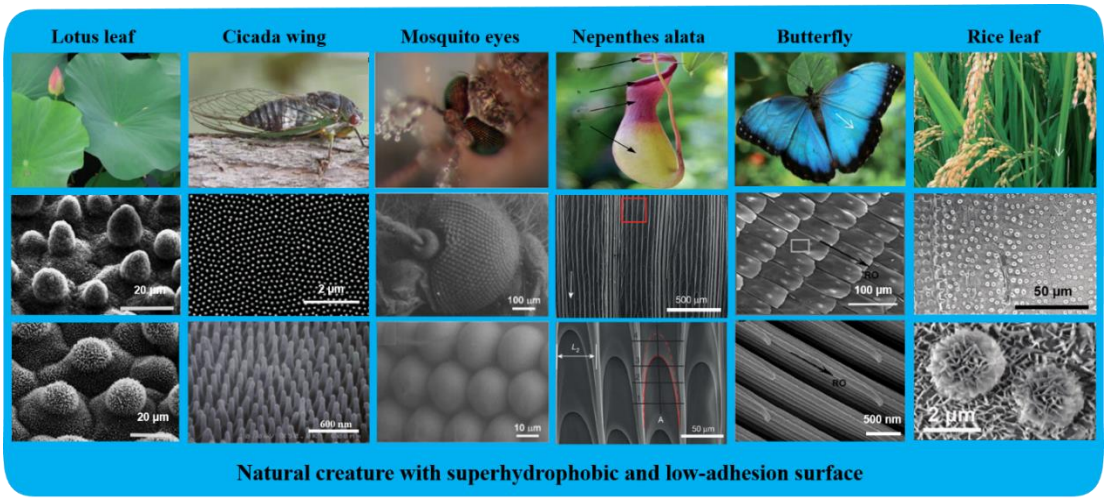

Figure 1. Natural creature with superhydrophobic and low-adhesion surface, including lotus leaf, reproduced with permission.[34] Copyright 1997, Springer-Verlag. Cicada wing, reproduced with permission.[35] Copyright 2012, Wiley-VCH Verlag GmbH & Co. KGaA. Mosquito eyes, reproduced with permission.[36] Copyright 2007, Wiley-VCH Verlag GmbH & Co. KGaA. Nepenthes alata, reproduced with permission.[37] Copyright 2016, Nature Publishing Group. Butterfly, reproduced with permission.[38] Copyright 2007, The Royal Society of Chemistry. Rice leaf, reproduced with permission.[39] Copyright 2013, Wiley-VCH Verlag GmbH & Co. KgaA.

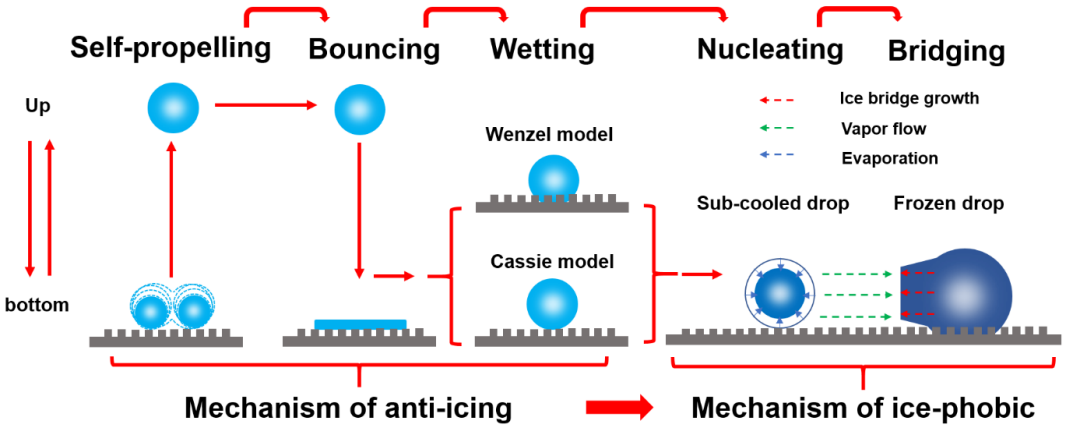

Figure 2. The mechanism of anti-icing and ice-phobic, including the process of self-propelling, bouncing, wetting, nucleating, and bridging.

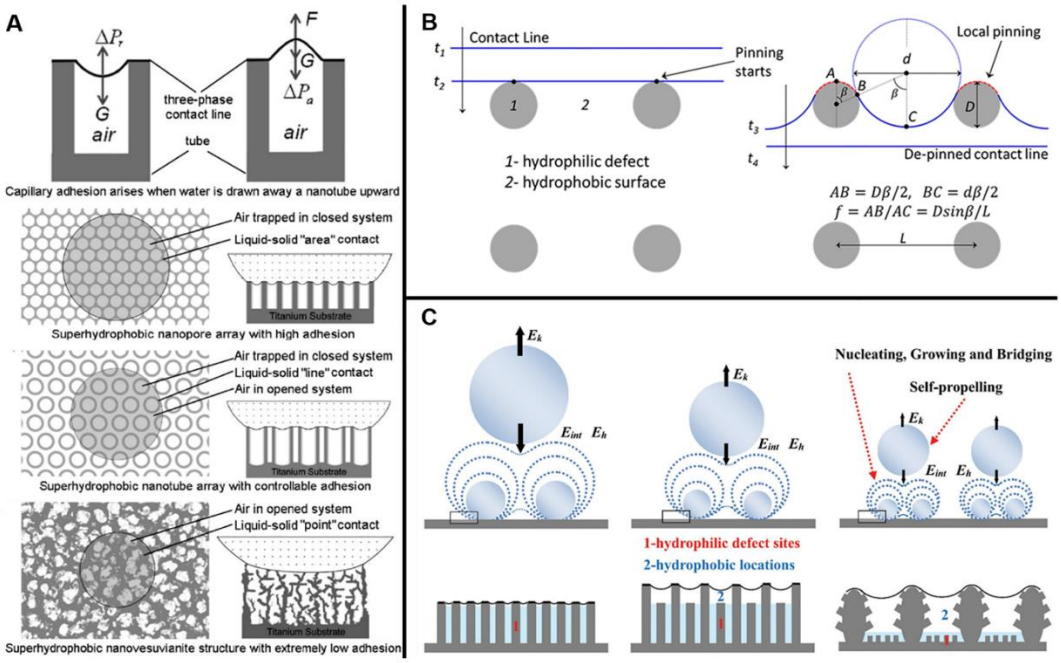

Figure 3. Mechanism of self-propelling: A) Schematic illustration of three types of superhydrophobic porous-nanostructure models with water adhesive forces ranging from high to low. Reproduced with permission.[56] Copyright 2009, WILEY-VCH Verlag GmbH & Co. KGaA. B) Schematic of the contact line movement (receding) on a background surface "2" with more wetting circular defects "1" in a square array.

Reproduced with permission.[57] Copyright 2012, American Chemical Society. C) Schematic illustrations of effect of three types of superhydrophobic samples with differently dynamic wettability on droplets' size and density. Reproduced with permission.[60] Copyright 2016, Wiley-VCH Verlag GmbH & Co. KgaA.

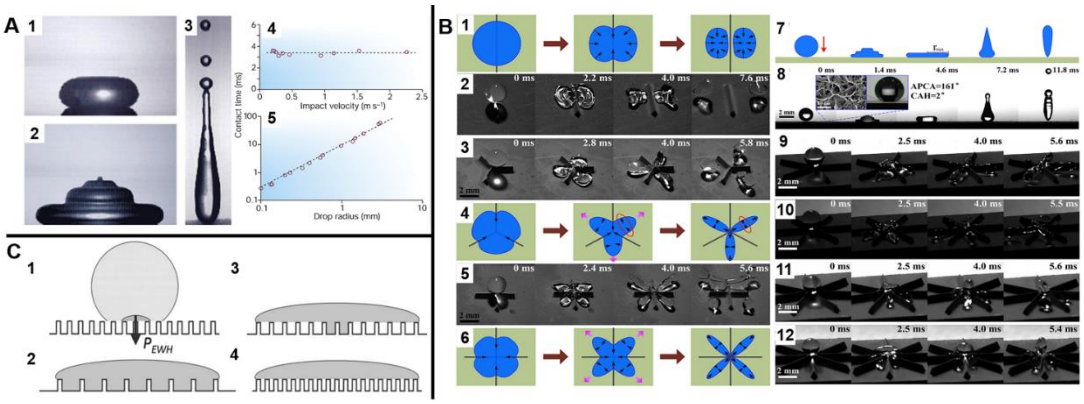

Figure 4. Mechanisms of drop bouncing. A) 1-3, the process of drop bouncing, 4-5, Contact time of a bouncing drop as a function of impact velocity and drop radius. Reproduced with permission.[115] Copyright 2002, Nature Publishing Group. B) The impact processes of water droplets on superhydrophobic surfaces with different macrotextures captured by a high-speed camera. Reproduced with permission.[124] Copyright 2015, AIP Publishing LLC. C) Relative magnitude of the wetting and antiwetting pressures decides the wetting states of impinging droplets. Reproduced with permission.[129] Copyright 2009, American Institute of Physics.

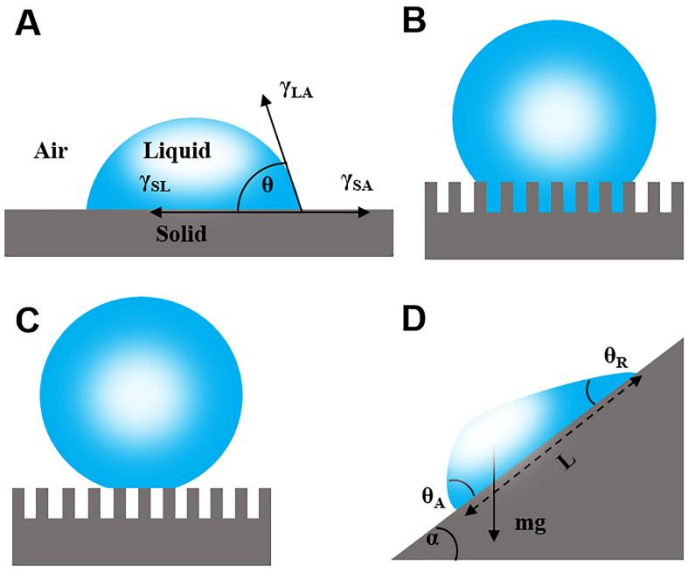

Figure 5. Model of wetting mechanisms. A) Young's equation. B) Wenzel model. C) Cassie model. D) Furmidge equation. Reproduced with permission.[41] Copyright 2016, Wiley-VCH Verlag GmbH & Co. KGaA, Weinheim.

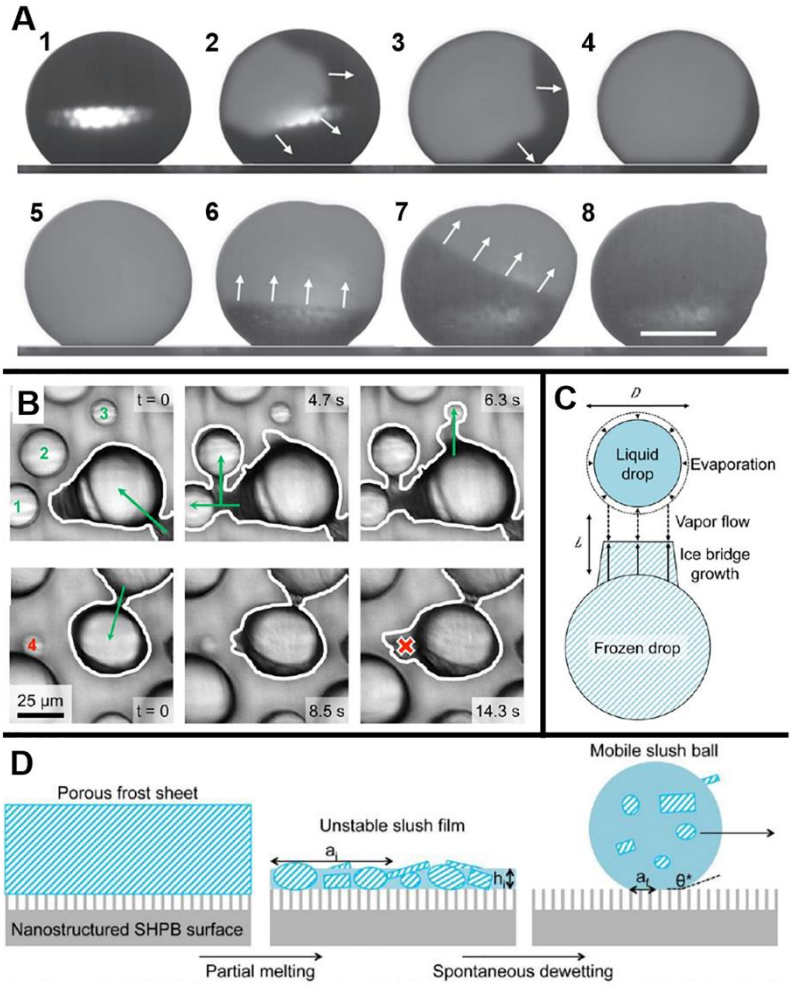

Figure 6. The mechanism of ice nucleation. A) The process of freezing of a supercooled water volume under shear flow. Reproduced with permission.[148] Copyright 2012, Macmillan Publishers Limited. B) Ice bridge growth from a frozen drop to neighboring liquid drops on a hydrophobic surface. C) Schematic of the growth of an ice bridge between a frozen drop and a subcooled liquid drop. Reproduced with permission.[84] Copyright 2013, American Chemical Society. D) Schematic of the dynamic defrosting process. Reproduced with permission.[155] Copyright 2013, American Chemical Society.

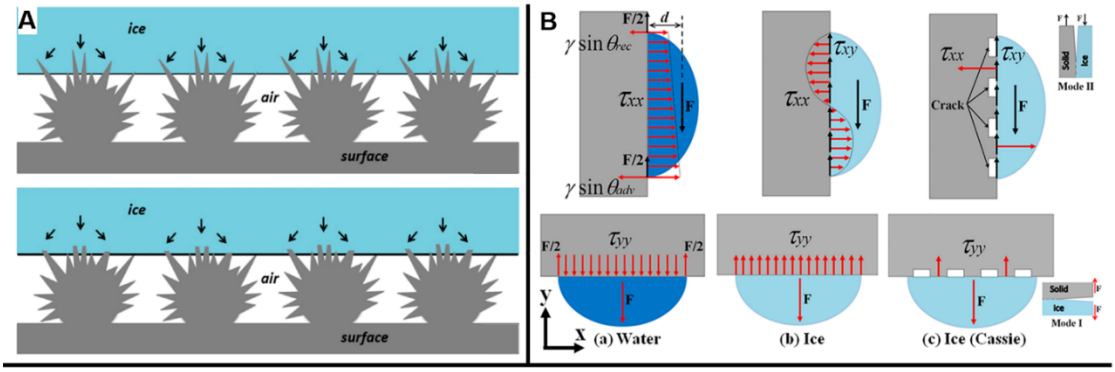

C | The comparison of the hydrophobicity and icephobicity

Property	Water	Ice
Definition of "phobicity"	Low surface energy/low adhesion High contact angle Low CA hysteresis Bouncing-off	Low adhesion Low normal strength (maximum stress) Low shear strength Bouncing-off supercooled droplets
Interaction	Hydrophobic interaction	Crystallization of ice and snowflakes
Thermodynamic relationship	Minimization of $\Delta G = \Delta H - T\Delta S$	Surface roughening transition $\Delta G = \Delta H - T\Delta S = 0$ and similar
Typical manifestation of the interactions	Hydrocarbone molecules in water environment	Ice molecules in saturated vapor environment at negative temperatures
Effects	Protein folding (including fractal shape), self-organized criticality, long-range hydrophobic force, wetting transitions	Snowlakes (diverse but symmetric, fractal)

Figure 7. Mechanism of ice adhesion. A) Schematic illustration of the surface structure with ice (up) and its damage caused by the icing/deicing processes (down). Reproduced with permission.[169] Copyright 2013, American Chemical Society. B) Normal (red) and shear (black) forces during shear loading of (a) water droplet and (b) ice frozen droplet on a flat and (c) textured surface in the regime of the tangential and normal loading. Reproduced with permission.[170] Copyright 2012, American Chemical Society. C) The comparison of the hydrophobicity and icephobicity. Reproduced with permission.[173] Copyright 2013, Macmillan Publishers Limited, part of Springer Nature.

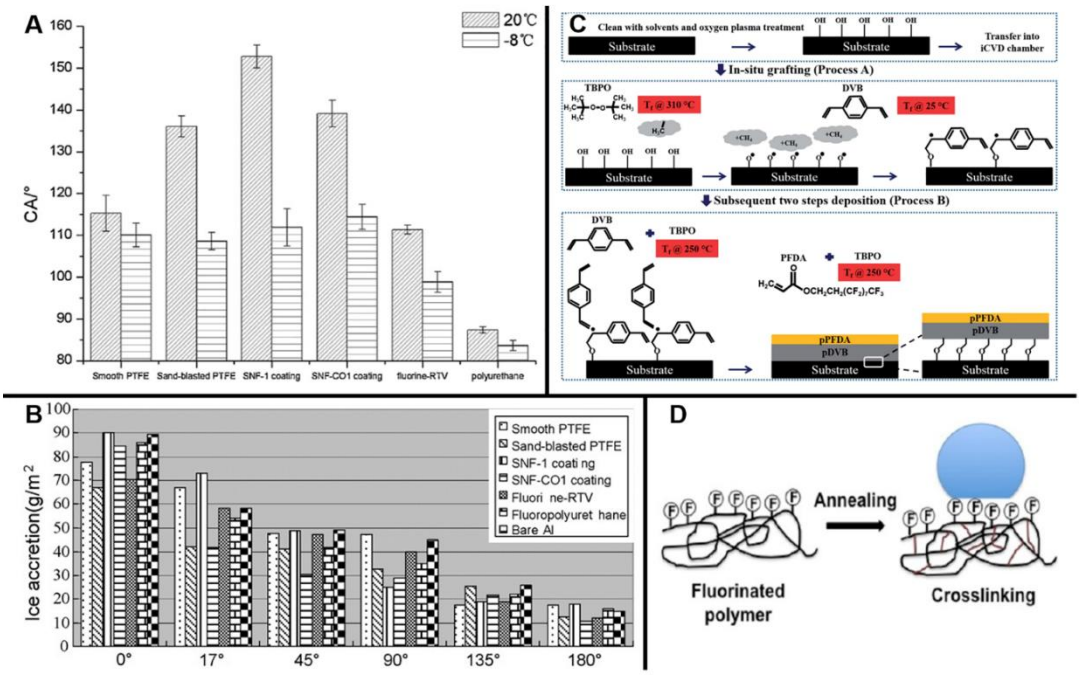

Figure 8. A) Contact angle of the fluoropolymer materials at different temperatures. Reproduced with permission. Copyright. B) Results of ice accretion of PTFE materials at different angles. Reproduced with permission.[184] Copyright 2011, Published by Elsevier B.V. C) Schematics of the substrate (silicon or steel) preparation, the in-situ linker-free grafting (process A), and the subsequent two-step polymer deposition (process B). Reproduced with permission.[185] Copyright 2015, The Royal Society of Chemistry. D) Schematics of cross-linking after an annealing treatment to the fluorinated polymer. Reproduced with permission.[186] Copyright 2013, American Chemical Society.

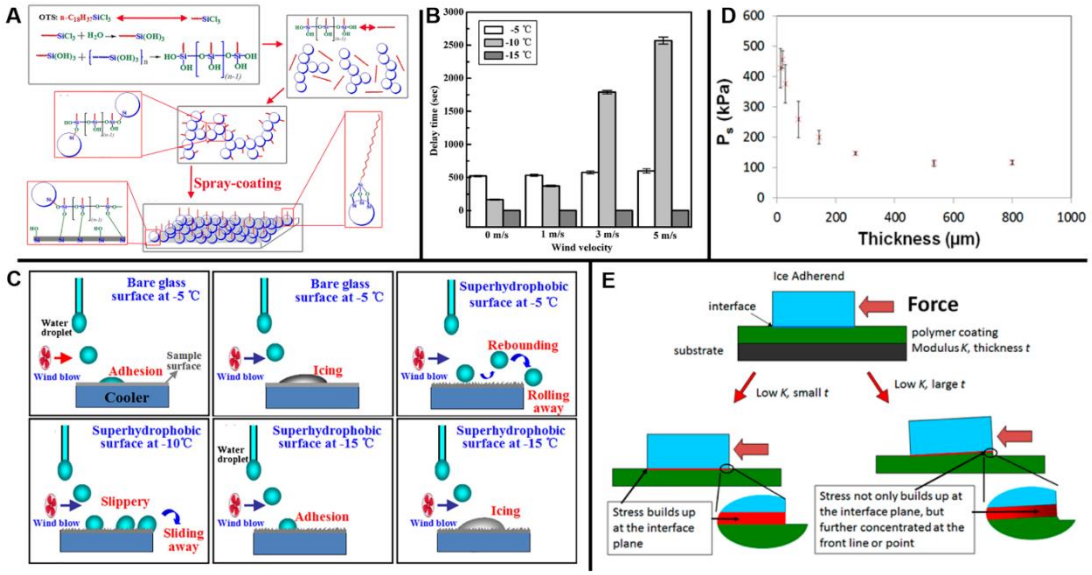

Figure 9. A) Schematic illustrations of synthesis silica sol solution and the preparation of silica coating by spray coating. B) Freezing delay time of water droplet on the superhydrophobic coating surface at different temperatures and wind velocities. C) Icing and anti-icing mechanisms of samples with different surface wettabilities at various temperatures under wind action. Reproduced with permission.[191] Copyright 2015, Springer Science+Business Media New York. D) Peak removal force in shear (Ps) as a function of coating thickness with 0.05 mm/s probe speed. E) Schematic diagram demonstration of stress building up at the interface plane and/or the front line or point during removal of a rigid, bonded object (ice) from a soft coating. Reproduced with permission.[192] Copyright 2014, American Chemical Society.

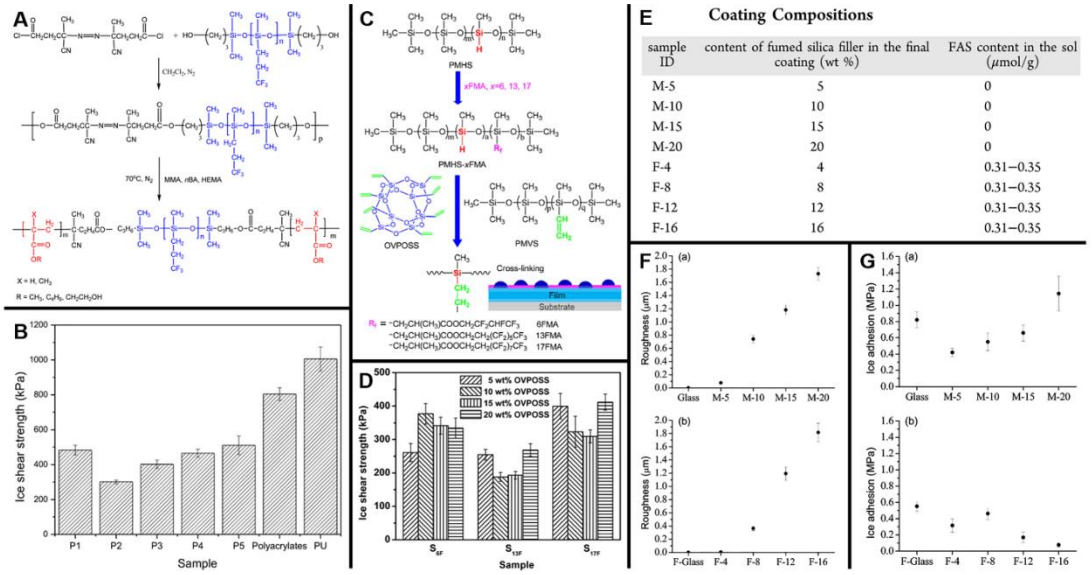

sample ID	content of fumed silica filler in the final coating (wt %)	FAS content in the sol (μmol/g)
M-5	5	0
M-10	10	0
M-15	15	0
M-20	20	0
F-4	4	0.31−0.35
F-8	8	0.31−0.35
F-12	12	0.31−0.35
F-16	16	0.31−0.35

Figure 10. A) Synthesis of fluorinated polymethylsiloxane (PMHS–xFMA) and formation of hybrid ice-phobic films from PMHS–xFMA and octavinyl-polyhedral oligomeric silsesquioxanes (OVPOSS) based on the addition reaction between vinyl group and Si-H group. B) Ice shear strength of the fluorinated polymethylsiloxane/OVPOSS hybrid films. Reproduced with permission.[193] Copyright 2014, Elsevier B.V. C) Synthesis of the PMTFPS–b-polyacrylate copolymers. D) Ice shear strength of PMTFPS–b-polyacrylate film. Reproduced with permission.[194] Copyright 2015, Elsevier B.V. E) Coating Compositions. F) Surface roughness of coatings: samples without addition of FAS (up); samples with FAS (down). G) Ice adhesion strength of coatings without FAS (up); with FAS (down). Reproduced with permission.[195] Copyright 2014, American Chemical Society.

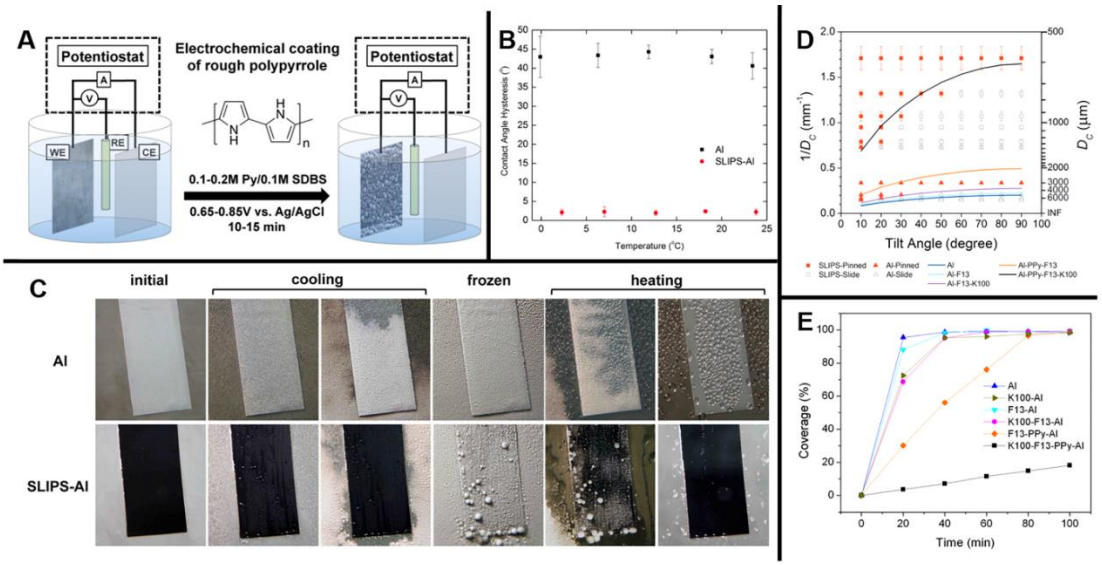

Figure 11. A) Schematics of the procedure for electrochemical coating of nanostructured polypyrrole on aluminum sheet. B) Contact angle hysteresis (CAH) of water on bare aluminum (Al) and SLIPS-Al measured at different temperatures. C) Comparison of still images about ice formation by deep freezing (-10 ℃) in high-humidity condition (60% RH) and subsequent deicing by heating. D) Droplet retention phase diagram for various aluminum surfaces tested. E) Fraction of the surface covered by ice on large aluminum samples as a function of cooling time at -2 ℃ and 60% RH. Reproduced with permission.[196] Copyright 2012, American Chemical Society.

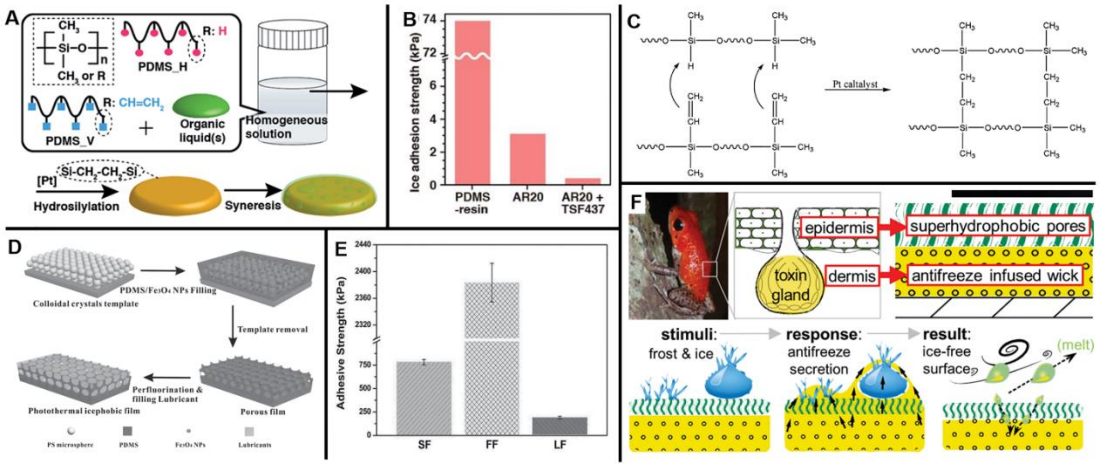

Figure 12. A) Conceptual scheme of gel formation and gelation-induced syneresis of organic liquids. B) Adhesion strength between ice and various organogels. Reproduced with permission.[197] Copyright 2015, The Royal Society of Chemistry. C) Curing Mechanism Based on the Pt Catalytic Addition Reaction between Vinyl Group in PDMS-V and Si−H Group in PDMS-H. Reproduced with permission.[198] Copyright 2013, American Chemical Society. D) Schematic procedures for fabricating photothermal ice-phobic film. E) The average ice adhesion strength on different films. Reproduced with permission.[199] Copyright 2015 WILEY-VCH Verlag GmbH & Co. KGaA. F) Schematic of the stimuli-responsive antifreeze secreting anti-icing coating inspired by the functionality and bilayer architecture of a poison dart frog skin (up), and schematic of the stimuli-responsive anti-freezing process (down). Reproduced with permission.[200] Copyright 2015, WILEY-VCH Verlag GmbH & Co. KGaA.

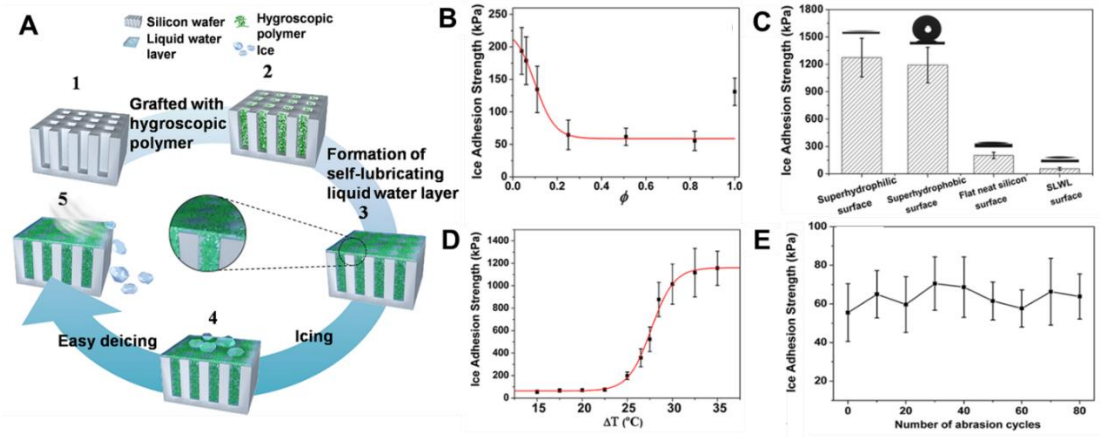

Figure 13. A) Schematic illustration of the preparation of the self-lubricating liquid water layer surface. B) Plots of the measured ice adhesion strength on the micropore arrayed silicon wafer surfaces impregnated with cross-linked hygroscopic polymers as a function of the area fraction, ϕ. C) Average ice adhesion strengths on four different test surfaces. D) Ice adhesion strength on the self-lubricating liquid water layer surface versus the supercooling. E) Average ice adhesion strengths on the anti-icing surface with self-lubricating liquid water layer remained almost the same after several tens cycles of abrasion test. Reproduced with permission.[201] Copyright 2013, American Chemical Society.

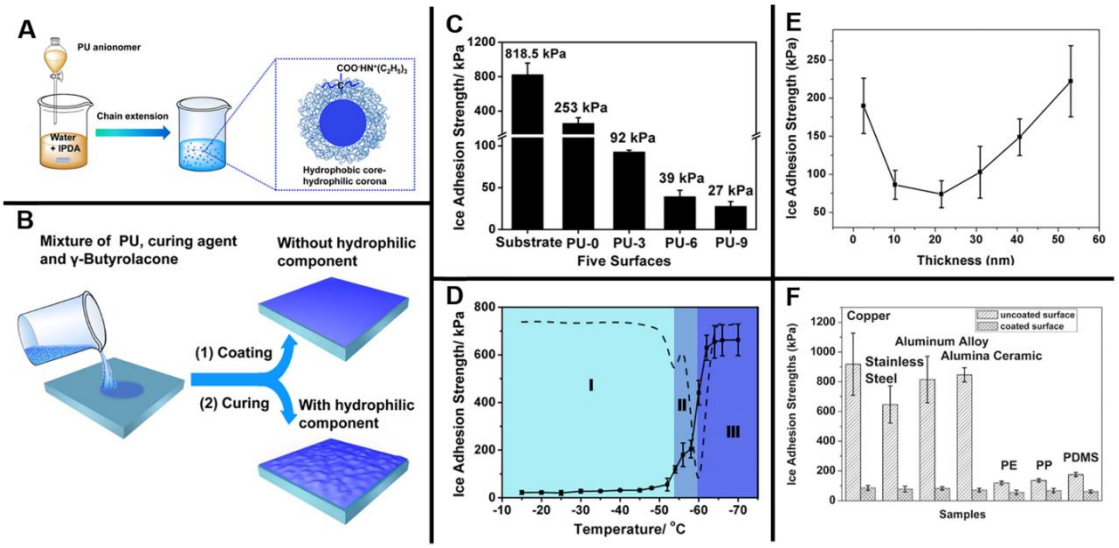

Figure 14. A) Preparation of the core−corona particles dispersion. B) Schematic illustration of the preparation of the anti-icing coating. C) Ice adhesion strength on PU coatings with different weight content of the hydrophilic component. D) Ice adhesion strength of PU-9 at different temperatures. Reproduced with permission.[203] Copyright 2014, American Chemical Society. E) Ice adhesion strengths on HA-D coated surfaces versus film thickness. F) Average ice adhesion strengths on the uncoated and coated surfaces measured at −15 °C. Reproduced with permission.[207] Copyright 2014, Wiley-VCH Verlag GmbH & Co. KGaA.

Songnan Zhang got his Bachelor of Textile Engineering from Hebei University of Science and Technology in 2013. He is currently pursuing his Doctor degree in College of Textile and Clothing Engineering at Soochow University. He is committed to nanomaterial fabrication and their corresponding application of superwettability in energy and environment.

Jianying Huang received her Ph.D. degree in 2007 from the Department of Materials, Xiamen University. During 2007–2011, she worked as an assistant professor at Fujian Institute of Research on the Structure of Matter. After that, she moved to Muenster University as a visiting scholar. She is currently an associate professor at National Engineering Laboratory for Modern Silk, and School of Textile and Clothing Engineering in Soochow University since 2013. Her research interests focus on the bio-inspired intelligent surfaces with superwettability, ATRP and click-chemistry reactions.

Yuekun Lai is a professor in the College of Textile and Clothing Engineering at Soochow University, with joint appointments in the National Engineering Laboratory for Modern Silk from 2013. He obtained his Ph.D. degree from the Department of Chemistry, Xiamen University. During 2009–2011, he worked as a research fellow at the School of Materials Science and Engineering, Nanyang Technological University, Singapore. In 2011, he moved to Muenster University under the support of the Humboldt Foundation Scholarship of Germany. His current research topics are bio-inspired intelligent materials with speical wettability, multifunctional fabrics, and TiO_2 nanostructures for energy & environmental applications.

Bioinspired from creatures, a series of the innovative fabrication technologies and anti-icing & ice-phobic materials with special wetting have emerged. Based on the anti-icing mechanism and ice-phobic mechanism, scientists found low-surface energy coatings and liquid-infused layered coatings can be effective to improve the efficiency of anti-icing & ice-phobic, which is significant for future development of the anti-icing & ice-phobic technology.

Keyword: wettability, anti-icing, ice-phobic, superhydrophobic (SHS), slippery liquid-infused porous surface (SLIPS)

Songnan Zhang, Jianying Huang, Yan Cheng, Hui Yang and Yuekun Lai*

Bioinspired Surfaces with Superwettability for Anti-icing & Ice-phobic Application: Concept, Mechanism, and Design